Computational and Structural Biotechnology Journal 19 (2021) 5072–5091

COMPUTATIONAL AND STRUCTURAL BIOTECHNOLOGY JOURNAL

journal homepage: www.elsevier.com/locate/csbj

Structural determinants of peptide-dependent TAP1-TAP2 transit passage targeted by viral proteins and altered by cancer-associated mutations

Monikaben Padariya [a,*,1], Sachin Kote [a], Marcos Mayordomo [a], Irena Dapic [a], Javier Alfaro [a,b], Ted Hupp [a,b], Robin Fahraeus [a,c,d,e,*], Umesh Kalathiya [a,*,1]

[a] International Centre for Cancer Vaccine Science, University of Gdansk, ul. Kładki 24, 80-822 Gdansk, Poland
[b] Institute of Genetics and Cancer, University of Edinburgh, Edinburgh, Scotland EH4 2XR, United Kingdom
[c] Inserm UMRS1131, Institut de Génétique Moléculaire, Université Paris 7, Hôpital St. Louis, F-75010 Paris, France
[d] Department of Medical Biosciences, Building 6M, Umeå University, 901 85 Umeå, Sweden
[e] RECAMO, Masaryk Memorial Cancer Institute, Zlutykopec 7, 65653 Brno, Czech Republic

ARTICLE INFO

Article history:
Received 31 March 2021
Received in revised form 6 September 2021
Accepted 6 September 2021
Available online 9 September 2021

Keywords:
Peptide
Transporters
MHC-I
Cancer mutations
Viral factors
Molecular dynamics
Kinetics
TAP1
TAP2
In silico peptide screening
Immunopeptidome
IFN-γ

ABSTRACT

The TAP1-TAP2 complex transports antigenic peptide substrates into the endoplasmic reticulum (ER). In ER, the peptides are further processed and loaded on the major histocompatibility class (MHC) I molecules by the peptide loading complex (PLC). The TAP transporters are linked with the PLC; a target for cancers and viral immune evasion. But the mechanisms whereby the cancer-derived mutations in TAP1-TAP2 or viral factors targeting the PLC, interfere peptide transport are only emerging. This study describes that transit of peptides through TAP can take place via two different channels (4 or 8 helices) depending on peptide length and sequence. Molecular dynamics and binding affinity predictions of peptide-transporters demonstrated that smaller peptides (8–10 mers; e.g. AAGIGILTV, SIINFEKL) can transport quickly through the transport tunnel compared to longer peptides (15-mer; e.g. ENPVVHFFKNIVTPR). In line with a regulated and selective peptide transport by TAPs, the immunopeptidome upon IFN-γ treatment in melanoma cells induced the shorter length (9-mer) peptide presentation over MHC-I that exhibit a relatively weak binding affinity with TAP. A conserved distance between N and C terminus residues of the studied peptides in the transport tunnel were reported. Furthermore, by adversely interacting with the TAP transport passage or affecting TAP_{NBD} domains tilt movement, the viral proteins and cancer-derived mutations in TAP1-TAP2 may induce allosteric effects in TAP that block conformation of the tunnel (closed towards ER lumen). Interestingly, some cancer-associated mutations (e.g. $TAP1_{R372Q}$ and $TAP2_{R373H}$) can specifically interfere with selective transport channels (i.e. for longer-peptides). These results provide a model for how viruses and cancer-associated mutations targeting TAP interfaces can affect MHC-I antigen presentation, and how the IFN-γ pathway alters MHC-I antigen presentation via the kinetics of peptide transport.

1. Introduction

Cytotoxic T lymphocyte response to infected or transformed cells depends on the presentation of peptide antigens on major histocompatibility complex class I (MHC-I) molecules. The majority of MHC-I presented peptides are generated in the cytosol by the proteasome and transported into the endoplasmic reticulum (ER) lumen for further processing by the ERAP aminopeptidases, before loaded onto MHC-I molecules by the dynamic multi-component assembly peptide-loading complex (PLC) (Fig. 1) [1–3]. PLC (Fig. 1) includes; TAP1 and TAP2 (transporter 1 and 2) heterodimer complex, MHC-I, β2microglobulin (β2m), the chaperones tapasin, calreticulin, and ERp57 (ER protein 57) [1–3]. The TAP transporters constitute functionally key components of the antigen presentation pathway since they link the cytosolic pool of peptides with the PLC and the ER-resident MHC-I molecules (Fig. 1) [1].

* Corresponding authors at: International Centre for Cancer Vaccine Science, University of Gdansk, ul. Kładki 24, 80-822 Gdansk, Poland (M. Padariya).
E-mail addresses: monikaben.padariya@ug.edu.pl (M. Padariya), robin.fahraeus@inserm.fr (R. Fahraeus), umesh.kalathiya@ug.edu.pl (U. Kalathiya).
[1] These authors contributed equally to this work.

https://doi.org/10.1016/j.csbj.2021.09.006

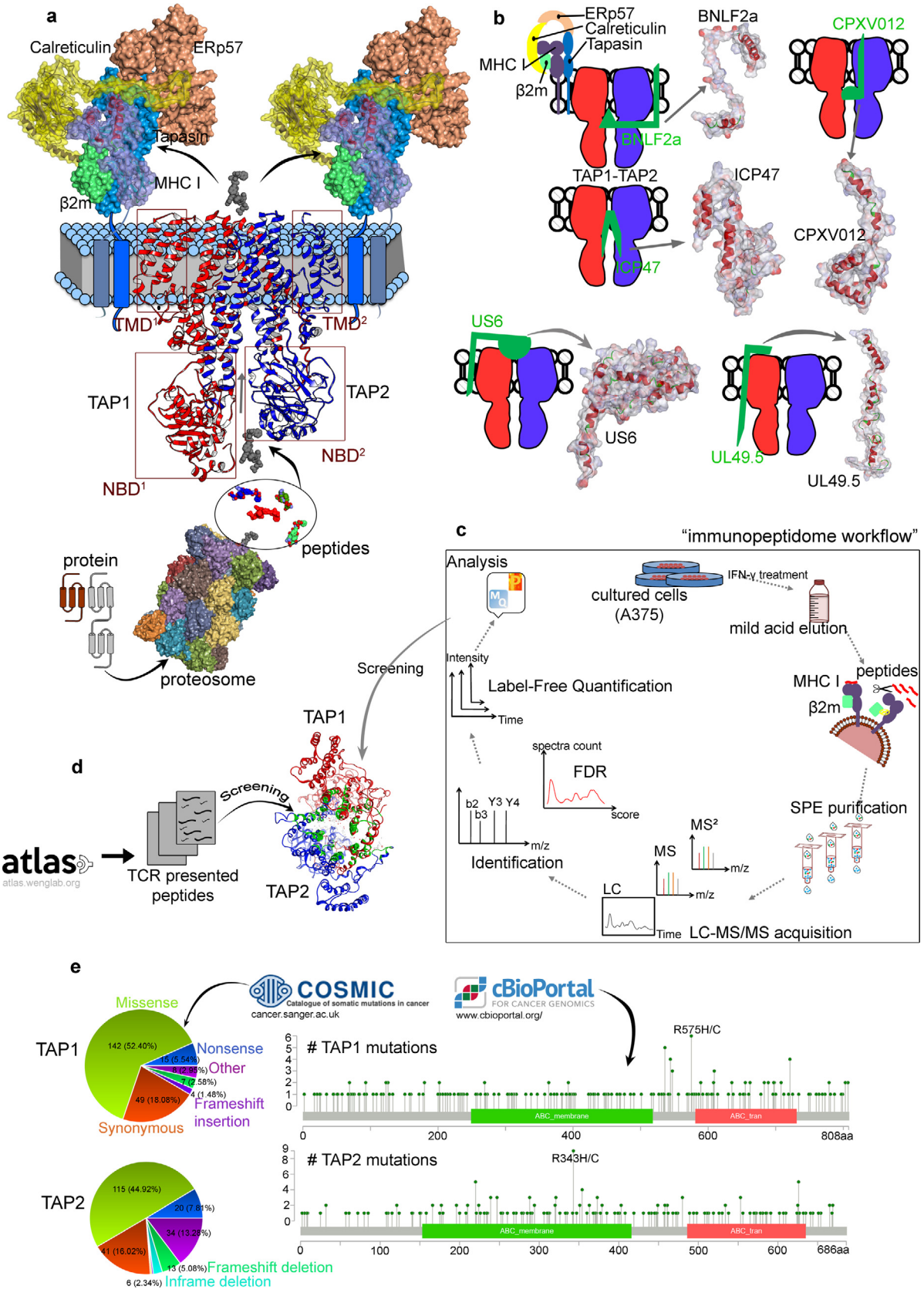
a
Calreticulin
ERp57
Tapasin
MHC I
β2m
TMD1
TMD2
TAP1
TAP2
NBD2
NBD1
peptides
protein
proteosome
b
ERp57
Calreticulin
Tapasin
MHC I
β2m
BNLF2a
CPXV012
TAP1-TAP2
ICP47
US6
UL49.5
c
"immunopeptidome workflow"
Analysis
cultured cells
(A375)
IFN-γ treatment
mild acid elution
Intensity
Label-Free Quantification
Time
MHC I
β2m
peptides
spectra count
FDR
score
b2
b3
Y3 Y4
m/z
Identification
SPE purification
MS²
MS
LC
Time
LC-MS/MS acquisition
Screening
d
atlas
atlas.wenglab.org
TCR presented
peptides
Screening
TAP1
TAP2
e
COSMIC
Catalogue of somatic mutations in cancer
cancer.sanger.ac.uk
cBioPortal
FOR CANCER GENOMICS
www.cbioportal.org/
TAP1
Missense
142 (52.40%)
Nonsense
15 (5.54%)
Other
8 (2.95%)
7 (2.58%)
4 (1.48%)
49 (18.08%)
Frameshift
insertion
Synonymous
TAP1 mutations
R575H/C
ABC_membrane
ABC_tran
808aa
TAP2
115 (44.92%)
20 (7.81%)
34 (13.28%)
41 (16.02%)
13 (5.08%)
Frameshift deletion
6 (2.34%)
Inframe deletion
TAP2 mutations
R343H/C
ABC_membrane
ABC_tran
686aa

The TAP transporters belong to the superfamily of ATP-binding cassette (ABC) transporters. Some of these transporters are associated with severe human diseases like cystic fibrosis [4,5], and they play major roles in multidrug resistance of pathogenic bacteria, reduced efficacy of antitumor drugs, cholesterol metabolism, cell homeostasis, and immune response [6]. Therefore, understanding the functional mechanisms of ABC transporters is important for therapeutic development. The TAP1 (ABCB2) and TAP2 (ABCB3) transporters, each have an N-terminal transmembrane domain (TMD) and a C-terminal nucleotide-binding domain (NBD) [7]. In the core part of the TMDs, the outer TM helices bind the other PLC component tapasin, the inner helices are responsible for peptide binding and form the channel, which mediates the peptide translocation [8,9]. Peptide binding to TAP is ATP-independent [10,11], whereas peptide transport from the cytosol to the ER requires ATP binding and hydrolysis [12]. The TAP_{NBDs} carry out the ATP hydrolysis to energize the conformational changes of the TMDs required for peptide translocation [1,12].

Substantial effort has been made to understand the peptides that are translocated by the TAP1-TAP2 transporters. Several biochemical studies have identified the nucleotide binding structural motifs, roughly mapped the peptide binding region, and provided the secondary structures responsible for the crosstalk between ATP hydrolysis in the TAP_{NBDs} and conformational changes of the TM helices [1,13]. However, the picture is still incomplete, as it has not been conclusively integrated into a robust trajectory of how the TAP dynamics and the substrates move to carry out a transport cycle. The precise conformational changes that occur as a result of substrate or nucleotide binding to TAP1/TAP2 are also not characterized [1]. The TAP transporters show a common fold with all structurally characterized ABC transporters [6,14]. Recent expansion of several new high-resolution transporter structures in different conformations produced many structural models of the TAP transporters [1,6,13,15–18]. Thus, the structural understanding of the TAP1-TAP2 complex is largely based on such extrapolations. However, it has also been suggested that the transporters most likely do not undergo the same structural cycles and no common mechanism has been proposed [1,14]. For this reason, the novel insights of TAP structures will be of importance.

Impaired TAP function results in reduced surface expression of MHC-I, as the empty MHC-I molecules are unable to present antigens to the immune system and is a common target for viral as well as cancer immune evasion [15,19–23]. Approximately, 15–20% of all human cancers worldwide are linked to viruses and this percentage could grow in the future [24]. MHC-I surface expression abnormalities have been identified in virus-associated cancers and non-cancerous cells, and thus, delineate a significant mechanism of virus infected cells to evade proper immune response. In most cases, this downregulation has been related to impaired TAP expression, which could be a result of structural alterations or dysregulation [25–28]. Several viruses have evolved factors that block the function of TAP [29], including herpesviruses such as Epstein-Barr virus, human cytomegalovirus, and herpes simplex virus type 1 that establish lifelong persistence in the host [30]. Association of these viruses with certain types of cancer or human malignancies has been demonstrated and knowledge about their targets, as well as functioning mechanisms can be useful in the development of future antiviral treatment strategies [31]. In concert with this, we investigated the TAP1-TAP2 transporters at the atomic level with a particular focus on how viruses inhibit TAP-mediated peptide translocation at a molecular level. The dynamics of the following TAP attacking viral immune evasion proteins were studied: BNLF2a from Epstein-Barr virus [32], CPXV012 from cowpox virus [33], ICP47 from herpes simplex virus type 1 [34,35], US6 from human cytomegalovirus [36], and UL49.5 encoded by varicellovirus [37].

To form a catalog of peptides likely to be transported by the TAP1-TAP2 complex, a systematic immunopeptidome workflow was applied as shown in Fig. 1c. Peptide loaded on the MHC molecules in melanoma cells were identified by acid elution followed by mass spectrometry (MS) analysis. The virus infected cells form one key model with which to analyze the response of the immune system, however, some viruses escape immune surveillance by altering and inhibiting the MHC-I presentation pipeline. An alternative way to mimic the parts of the cellular immune response that occurs during viral infection can be to treat cells with interferons (IFNs) [39,40]. Interferons are important cytokines, produced in response to viral infection, alert the immune system, and enhance cellular response to the infection (increase the presentation of MHC molecules) [41]. Thus, analyzing the effect of IFNs on the MHC-I immunopeptidome in cultured human cells can provide a model for examining the effects of viral infection on the MHC peptidome [40]. The type I (IFN-α and IFN-β) and type II (IFN-γ) IFNs are key cytokines in the antiviral response. IFN-β is secreted from most cells in response to viral infection involving dendritic cells and many other cell types in the body [40,42]. At later stages of immune response, IFN-γ is secreted from T-cells and other immune cells [40]. The interferons strongly affect cellular metabolism and gene expression, including MHC-I as well as MHC-II molecules and also upregulate antigen processing and presentation components such as; ER aminopeptidase 1/2 and the TAP transporters [8,40,42,43,44–46]. Moreover, when cells are treated with IFN-γ, the regular proteasomes are replaced by the immunoproteasomes [46]. This replacement has been associated with an enhanced immune response and the peptides produced by immunoproteasomes mainly contain hydrophobic or basic C termini, which are preferred substrates for the TAP transporters and

Fig. 1. The TAP1-TAP2 transporters molecular and structural aspects in the peptide-loading complex. (a) The modeled tertiary structures of TAP1-TAP2 heterodimeric transporters, including the N-terminal transmembrane domains (TMD) that were found missing in the cryo-EM structure (pdb id.: 5u1d) [18,23]. Antigenic peptide presentation by MHC-I begins with the degradation of cytosolic proteins into peptides by the proteasome, which are then transported across the ER membrane by the TAP transporters. Followingly, the peptides can be loaded over the surface of the MHC-I molecules residing in the peptide-loading complex (PLC), accommodated with several other components; β2m, ERp57, tapasin, and calreticulin [1–3]. (b) Viral immune evasion proteins interacting with the TAP transporters. ICP47 binds to TAP from the cytosol and inhibits the peptide binding, US6 blocks ATP binding to TAP by interfering from the ER lumen, UL49.5 blocks TAP dependent peptide transport and also catalyses the degradation of the PLC. BNLF2a binds to the core TAP structure and arrest it in a transport-incompetent conformation, CPXV012 inhibits TAP dependent peptide translocation, and thus, interfere with the MHC-I-peptide assembly in the ER [38]. Cryo-EM structure of human TAP with ICP47 (pdb id.: 5u1d) [18,23] was used as a template to model other TAP binding viral proteins BNLF2a, CPXV012, UL49.5, and US6. Three dimensional (3D) structures of viral protein are shown in ribbon representation with molecular surfaces. (c) The outline of the immunopeptidome workflow, representing the sample preparation to peptide identification protocol. (d) Datasets of TAP transported peptides retrieved from the ATLAS (Altered TCR Ligand Affinities and Structures) database (http://atlas.wenglab.org/). The peptides present in the crystal structure of TCR(T cells receptor)-peptide-MHC complexes were collected. In the 3D-structure of TAP, the defined active site for peptide screening is highlighted as green ribbons, red spheres represent hydrophilic and white sphere hydrophobic likeliness of the active site. (e) Cancer-associated mutations retrieved from the COSMIC (Catalogue of Somatic Mutations in Cancer; cancer.sanger.ac.uk) and cBioPortal (https://www.cbioportal.org/) databases for the TAP transporters. The pie chart from COSMIC represents different types of mutation with a number of samples labeled, as well as the percentage (%) of mutation covered. The scattered plot from cBioPortal, represents cancer mutations for TAP1 and TAP2 proteins along with its frequency. (For interpretation of the references to color in this figure legend, the reader is referred to the web version of this article.)

also appear to be more efficient at binding to MHC-I [8,40,43]. Consequently, immunoproteasomes are believed to enhance the MHC-I antigenic peptide generation and presentation [47]. Addditionally, the enhancement of MHC presentation by IFN treatment may add neoepitopes to the presented peptidome that can induce even stronger immune responses [40].

Moreover, we were interested to identify or trace if the transport of peptides through the TAP is affected or altered upon IFN-γ treatment. IFN-γ is known to induce the immunoproteasome with a different protease composition and to alter the length as well as cleavage sites of peptides.. The A375 cells were treated with IFN-γ, and the peptides were identified using mass spectrometry. Detected peptides were further *in silico* screened with the TAP1-TAP2 model, to investigate the peptide transport process from the cytosol to the ER via the TAP transporters. Additionally, to extend our analysis, a set of peptides from the ATLAS (Altered TCR Ligand Affinities and Structures) database (http://atlas.wenglab.org) were compiled, which are known to be presented on TCR as well as the structures of TCR-peptide-MHC complexes are known [48]. Interactions of these peptides with the TAP1-TAP2 complex were analyzed, along with tracing protein-peptide binding affinities.

The cancer-associated mutations and viral proteins may shares a common trend towards TAP transporters, which is attenuation of their activity. Defective TAP transporters in few tumor tissues have been identified by down-regulation of TAP mRNA or mutations. It has been proposed that by inducing a TAP attenuation mechanism the tumor cells escape immune response [15], and similarly, by down-regulating TAP1 levels, along with reducing MHC-I cell surface expression, the HPV (human papillomavirus) virus evades immune recognition [49,50]. Several studies have linked TAP transporter polymorphisms and the risk for the high-grade cervical intraepithelial neoplasia (CIN), cervical cancer, and pulmonary tuberculosis [150]. Einstein et al. suggest that the TAP1 I333V and TAP1 D637G mutations reduce a high-grade CIN [49,50]. The review by Rupert et al. highlighted defects in the TAP1 or TAP2 transporters can be the cause of bare lymphocyte syndrome (BLS) I, and during the viral infection the patients with BLS lacked increased susceptibility [51]. Ozbas-Gerceker et al. applying the PCR-RFLP (restriction fragment length polymorphism) method determined that polymorphism in $TAP1_{-333}$ and $TAP2_{-565}$ can be associated with multiple myeloma-MM and chronic lymphoid leukemia-CLL, respectively [52]. Moreover, the $TAP2_{-665}$ GG genotype could be a risk factor for different hematological malignancies [52]. The study of immunohistochemical expression of TAP1 and TAP2 in breast cancer patients suggested that their overexpression could be the cause of an aggressive breast tumor [53].

Therefore, to analyse the effects of somatic mutations on the TAP1 and TAP2 transporters, a large number of mutational hotspots for TAP1 and TAP2 genes were retrieved from the Catalogue of Somatic Mutations in Cancer (COSMIC, https://cancer.sanger.ac.uk/cosmic) [54], and cBio Cancer Genomics Portal (cBioPortal, http://cbioportal.org) databases [55]. Effects of point mutations on TAP1-TAP2 plasticity were determined by stability and binding affinity changes with respect to each other. In addition, the TAP1 and TAP2 genes were further investigated considering the single nucleotide polymorphism (SNPs) as well as the number of mutations that have been distributed within the human population. The regions in the TAP1-TAP2 transporters exposed bind to different viral proteins and were analysed in terms of the frequency of mutations or SNPs in those regions. Recently, a proteasome-dependent, but TAP-independent pathway has been described, showing that the well-known SIINFEKL peptide (the classical peptide epitope from ovalbumin presented by the MHC-I) can be imported into purified phagosomes in an ATP-dependent but TAP-independent manner [9,56–58]. Considering this fact, SIINFEKL peptide was also included with the TAP transporters as model for 8-mer peptides, as well as to make a comparative analysis with other studied peptides. To analyse the molecular consequences of cancer driving mutation and peptide binding with TAP1-TAP2 complex, the functionally important mutations and a set of peptides were further assessed by molecular dynamics simulations (MDS) [59].

2. Materials and methods

2.1. Experimental design and the sample preparation

2.1.1. Cell culture with the treatment of IFN-γ, as well as peptide isolation by mild acid elution

The melanoma A375 cells were previously described [60], and these A375 p53-wild-type status cells were grown in DMEM (Dulbecco's Modified Eagle's Medium) medium (invitrogen) supplemented with 10% heat-inactivated fetal bovine serum, 1% penicillin/streptomycin (invitrogen), and incubated at 37 °C with 5% CO_2. The parental A375 cells were grown over 10 cm diameter plates, and for the treatment cells were exposed to 100 IU/ml IFN-γ for 24 h. Following the protocol described in [61], mild acid elution (MAE) was performed with citrate phosphate pH 3.3 buffer. Biological replicates of 50×10^6 cells from both conditions (with and without IFN-γ treatment) were used. MHC associated peptides were released by MAE, using 1.5 mL of citrate phosphate buffer at pH 3.3 for the 50×10^6 cell samples. Cell suspensions were then pelleted and the resultant supernatants were considered as MHC-I peptides samples for further purifications. Followingly, the peptide sample extracts were desalted using Oasis HLB cartridges (30 mgs; water). Finally, the bound material was eluted with 1 mL H_2O/80% methanol (MeOH)/0.2% formic acid (FA) v/v, and diluted to H_2O/40% MeOH/0.2% FA v/v. Peptides were loaded on ultrafiltration devices (Microcon-10 kDa centrifugal filters, Millipore) to isolate peptides <10,000 Da, and remove higher molecular weight proteins. The resulting flow through content peptides was dried using vacuum centrifugation, which were then stored at −80 °C until MS analysis.

2.1.2. Mass spectrometry and the peptide sequencing

Vacuum dried MHC presented peptides were reconstituted in 30 μL of loading buffer composed of 0.08% trifluoroacetic acid (TFA)/2.5% acetonitrile (ACN) (v/v). Further, these peptides were analyzed by LC-MS/MS (Liquid chromatography–mass spectrometry cells) using an Ultimate 3000 nanoLC system coupled online to an Orbitrap Exploris 480 mass spectrometer (both from Thermo Fisher Scientific). The peptide samples (6 μL) initially were loaded onto μ-precolumn (C18 PepMap 100, 5 μm, 100 Å) 300 μmi.d. × 5 mm length cartridge trap column (P/N 160454, Thermo FisherScientific) for 10 min at a 5 μL/min flow rate. Peptides were separated on a C18 reversed-phase analytical column (C18 PepMap 100 RSLCnano column) 75 μm, i.d. × 150 mm length, 2 μm, 100 Å (P/N 164534, Thermo FisherScientific). LC solvents were composed of 0.1% FA in water (v/v) (solvent A) and 0.1% FA in water with 80% ACN (v/v/v) (solvent B). Peptides were eluted over a nonlinear gradient of 2.5–35% and 35–60% of B for 80 min and 15 min, respectively, at a flow rate of 300 nL/min controlled by the Ultimate 3000 nanoLC system. Finally the column was washed with 95% B for 10 min. Samples were analyzed in data-dependent acquisition (DDA) mode with the following settings; survey scan (MS1) range was set to 300 to 1650 m/z with a resolving power of 120,000 (at 200 m/z) and an AGC target value of 300% with a maximum injection time of 100 ms. Data was acquired with the data-dependent "top20" method, isolating the 20 most intense ions and fragment them by higher-energy collisional dissociation

(HCD) with applied normalized collision energy 30%. MS/MS resolution was 60,000 (at 200 *m*/*z*), AGC target value of 100% with a maximum injection time of 100 ms. For the MHC-I presented peptides, in case of unassigned precursor ion charge states, or charge states of four and above, no fragmentation can be performed. Dynamic exclusion of fragmented *m*/*z* values from the further selection set for the 20 s, and inject 6 μL of the first sample again (for technical duplicate). Followingly, the system was washed with two standard wash runs, before loading any next biological sample.

2.1.3. Peptide identification and label-free quantification

The database quests were implemented adopting the MaxQuant package (version 1.6.12.0) [62,63], to search the peak list against the human UniProt (www.uniprot.org) database (downloaded on 12.08.2020 consisting of 75,093 entries) using the built-in Andromeda search engine [64]. Mass tolerances for precursor and product ions were set to 20 ppm and 0.02 Da, respectively. Searches were performed without enzyme specificity and variable modifications for deamidation (N, Q) and oxidation (M). Possible sequence matches were restricted to 7–25 amino acids (aa), the mass of a maximum peptide of 4600 Da. The initial allowed mass deviation of the precursor ion to 10 ppm, and the maximum fragment mass deviation was set to 10 ppm. Further, the statistical analysis was performed with Perseus software (version 1.6.10.45). The FDR (false discovery rate) level was 5%, and protein abundance calculated using normalized spectral protein intensity (LFQ intensity; label-free quantification) on MaxQuant software, as previously described [65]. LFQ intensity values were set as Log2 transformed, and peptide groups quantified in all runs were considered for further analysis.

2.2. Peptide structure optimization and their binding affinities with the TAP1-TAP2 transporters

2.2.1. TAP transporters, peptides, and the viral factors model generation

Adopting the "Hidden Markov method" implemented in the Phyre2 server (http://www.sbg.bio.ic.ac.uk/phyre2) sequence alignments with the known protein structures were generated and based on the principles of homology modeling [66,67], the derived alignments were used to generate full protein tertiary structures. The intensive mode of Phyre2 successfully inserted the lacking segments in the TAP1, TAP2, and ICP47 structures (pdb id.: 5u1d) [18,23], as well as generated the complete modeled tertiary structures of BNLF2a, CPXV012, UL49.5, and US6 viral factors. Based on the percentage identity and alignment coverage the following templates were selected to model the proteins structures: TAP1 (pdb id.: 5u1d-chain A and 5yke-chain B), TAP2 (pdb id.: 5u1d-chain B and 5ykf-chain-H), ICP47 (pdb id.: 5u1d), BNLF2a (pdb id.: 5zaz), CPXV012 (pdb id.: 2lq0), UL49.5 (pdb ids.: 6qan and 6qbj), and US6 (pdb id.: 1otc). The resulting modeled structures were subjected to energy minimization in Molecular Operating Environment (MOE; Chemical Computing Group Inc., Montreal, QC, Canada) [68] applying the CHARMM27 forcefield [69]. Furthermore, the tertiary structures for the 3957 peptides from immunopeptidome analysis (with and without IFN-γ treatment), peptides from ATLAS (Altered TCR Ligand Affinities and Structures) database [48], and SIINFEKL peptide [56] were constructed and energy minimized using the homology modeling algorithms incorporated in the MOE (Chemical Computing Group Inc., Montreal, QC, Canada) package. Relaxed modeled structures of the peptides, TAP transporters, and viral proteins were subsequently used in the protein–protein or protein-peptide docking pipelines.

2.2.2. Protein-protein docking, in silico point mutation, and virtual screening of peptides with the TAP transporters

The rigid body docking protocol from the MOE (Chemical Computing Group Inc., Montreal, QC, Canada) [68] was used to achieve the complexes of TAP1-TAP2 with each viral protein inhibitor (ICP47, BNLF2a, CPXV012, UL49.5, and US6). The CHARMM27 forcefield [69] was used for energy minimization, 500 conformations per protein–protein docking were generated and ranked or scored using the Generalized Born/Volume Integral (GB/VI, kcal/-mol) [70] binding energies. Followingly, the refinement step based on molecular mechanics was carried out to analyse the best 100 poses of individual viral protein with the TAP1-TAP2 complex.

Peptides identified in the immunopeptidome analysis from the melanoma A375 cells (with and without IFN-γ treatment), and other 57 antigenic peptides (56 from ATLAS database [48] and SIINFEKL [56]) were screened against the TAP1-TAP2 complex using the MOE package (Chemical Computing Group Inc., Montreal, QC, Canada). The binding site in the TAP transporters for each peptide was identified through the "MOE site-finder" module, which computes the putative binding sites in a protein structure using a geometric approach with additional physico-chemical information such as; polarity or charge [68,71–72]. The "Alpha Shapes" construction [68,72] geometric method was used to compute the possible residues that can be considered for peptide docking to the pocket formed by the TAP1-TAP2 transporters. Following the determination of potential peptide binding sites in the TAP1-TAP2 complex, the protein-peptide docking was performed using the MOE (Chemical Computing Group Inc., Montreal, QC, Canada) package applying the CHARMM27 forcefield [69]. The MOE (Chemical Computing Group Inc., Montreal, QC, Canada) docking architecture formulates four different components involving; the generation of ligand-conformation, optional pharmacophore filtering, ligand placement with its scoring in the pocket, and flexible/-rigid receptor and ligand refinement with re-scoring. For placement of peptide in the TAP1-TAP2 complex, the "Triangle Matcher" protocol was applied (the optimized TAP structures were defined as rigid, whereas the peptides were set as flexible allowing their structures a high degree of freedom) [68,72]. Peptides are placed by superposing triplets of peptide atoms and triplets of receptor site points; the poses that clash with the protein were subsequently removed. To treat peptide flexibility in the protein-peptide molecular docking, 1000 conformations of each peptide were produced from their placement in the TAP binding site and the resulting complexes were evaluated using the GBVI/WSA dG (kcal/mol) binding affinity scoring [70,73], a forcefield based scoring function that calculates the free energy of binding of the peptide from a given position. Particularly, for the dataset containing 3957 immunopeptidome peptides, the best 5 optimized poses as ranked by binding affinity (GBVI/WSA dG) with the TAP were stored, and for the 57 peptides retrieved from the available crystal structures, the top 10 poses were saved. Furthermore, these best peptides influencing the binding energies and interactions with TAP proteins were considered for further evaluations.

Cancer derived mutations in the TAP1 and TAP2 proteins were subjected to the "Sequence Design" protocol of the protein design module in the MOE (Chemical Computing Group Inc., Montreal, QC, Canada) package. This pipeline computes the frequency with probability of amino acids at the residual mutation sites (mutation expression) [72]. The goal was to obtain the stability or binding affinity trade-offs, when peptide binds to wild-type and the mutated TAP transporters. In addition to applying this approach, all cancer hotspot residues were mutated using 20 other amino acids [A, R, N, D, C, Q, E, G, H, I, L, K, M, F, P, S, T, W, Y, and V]. The structural model for each single mutation was generated, the energy window was set to 10 kcal/mol, RMSD limit was 0.25 Å, and residues farther than 4.5 Å were kept fixed. The "LowMode

MD" was used with default parameters to produce a thorough conformational ensemble [74]. The resultant TAP mutations significantly affecting the stability and peptide binding affinity, were further selected for the MD simulations [59].

2.2.3. Single nucleotide polymorphisms in the TAP1 and TAP2 genes

The Genome Aggregation Database (gnomAD) [75], an online resource containing genome and exome sequencing variants from diverse projects and investigators, was used in order to detect the distribution of the SNPs (single nucleotide polymorphisms) across the TAP1 and TAP2 genes. Variants of these genes were downloaded in CSV format and processed in R environment (version 3.6.3), using the g3viz package to plot the protein modifications occurring downstream of the genome mutations.

2.2.4. The molecular dynamic simulations and system setup

Initial orientation of the wild-type or mutant TAP1-TAP2 transporters embedded in the membrane, and in complex with peptide or the viral protein was defined using the PPM server (https://opm.phar.umich.edu/ppm_server) [76]. Optimizing the free energy of transfer from water to the membrane environment, the PPM server thoroughly cross-verify dozens of transmembrane and peripheral proteins and peptides [76]. Resulting positioned complexes were used as an input for the CHARMM-GUI membrane builder (http://www.charmm-gui.org/?doc=input/membrane.bilayer) [77], to prepare the membrane-embedded complexes. The CHARMM-GUI platform provides a series of CHARMM inputs necessary to generate membrane embedded complexes for MD simulations [77]. The supramolecular PLC is expressed in the endoplasmic reticulum, and the TAP1-TAP2 resides in the ER membrane to transport the peptide across the membrane [78]. Thus, to better understand the protein dynamics in the membrane environment, TAP complexes were embedded in a membrane containing 660 palmitoyloleoyl phosphatidylcholine (POPC) lipids and 66 cholesterol molecules [79], accommodating the larger separation of TAP_{NBDs}. The membrane composition was evenly distributed throughout both leaflets of the bilayer. Other parameters applied were; rectangle box type, tetragonal crystal type, and a water thickness of 22.5 Å on the top as well as on bottom of the system. A heterogeneous lipid bilayer was generated using the replacement method [77,80], and the distance-based algorithm was used as an ion-placing method. The following 24 TAP-membrane complexes were further investigated using the MD simulation technique: apo-form (TAP1-TAP2 and pep18-alone), with viral protein (TAP1-ICP47-TAP2, TAP1-BNLF2a-TAP2, TAP1-CPXV012-TAP2, TAP1-UL49.5-TAP2, and TAP1-US6-TAP2), with peptides (TAP1-SIINFEKL-TAP2, TAP1-pep18-TAP2, TAP1-pep20-TAP2), with mutations ($TAP1_{E446K/W}$-TAP2, $TAP1_{V437F/I}$-TAP2, $TAP1_{R372Q}$-TAP2, TAP1-$TAP2_{D370N/W}$, TAP1-$TAP2_{G208F/S}$, and TAP1-$TAP2_{R373H}$), and mutation + peptide ($TAP1_{R372Q}$-pep18-TAP2, $TAP1_{R372Q}$-SIINFEKL-TAP2, TAP1-pep18-$TAP2_{R373H}$, and TAP1-SIINFEKL-$TAP2_{R373H}$).

The MD simulations were performed using the NAMD package [81] with CHARMM36 forcefield [82–84], and the TIP3P [85] water model. The particle-mesh Ewald method [86] was used to treat long-range electrostatics with a grid spacing of 1 Å, and a cut-off of 12 Å was used for van der Waals interactions. The force based switching was used with a switching distance of 10 Å. Periodic boundary conditions (PBC) were applied with constant pressure and temperature (NPT) ensemble to avoid finite size effects. Langevin dynamics [87] was used to maintain constant temperature with a damping coefficient of 1 ps^{-1}. The Nose-Hoover Langevin piston method [88] was applied to control the constant pressure with a decay period of 50 fs with a damping timescale of 25 fs. SHAKE algorithm [89] with a time step of 2 fs was used to constrain all the non-polar bonds involving hydrogen atoms. Equilibration of the system was performed for 10 ns at 303.15 K and the equilibrated systems were subsequently used to perform MD production runs for 100 ns at 303.15 K. The visual molecular dynamics (VMD) [90], MOE (Chemical Computing Group Inc., Montreal, QC, Canada), and BIOVIA Discovery Studio visualizer (Dassault Systèmes, BIOVIA Corp., San Diego, CA, USA) packages were used to analyse the molecular dynamics trajectories.

3. Results and discussions

A systematic immunopeptidome workflow was implemented, and a set of peptides presented over the MHC-I molecules in the melanoma A375 cells were isolated (Fig. 1c). Based on the sequences of the MHC-I bound peptides, their tertiary structures were generated using the homology modeling techniques; in order to analyse the pattern of binding as well as peptide translocation through TAP transporters. Furthermore, the binding and dynamics of viruses with TAP complex as well as the cancer mutations targeting the TAP transporter process were analyzed.

3.1. Human melanoma cells immunopeptidome, and screening of peptides against the TAP transporters

The melanoma A375 cells were grown *in vitro* under typical cell culture conditions, and the cells characterized with and without IFN-γ treatment in order to define the IFN-γ induced changes on the MHC antigen processing and presentation pathway (Fig. 1c). The distribution and length of the identified peptides from the both conditions (Fig. 2a and Tables S1–S3), suggest that there were more peptides identified in the IFN-γ treated cells (3081 peptides, Table S1) compared to that of the non-treated (termed as wild-type in this study) cells (1968 peptides, Table S2). About 1104 peptides were common in IFN-γ treated and non treated samples, whereas 1974 peptides were found on IFN-γ treated cells and 863 peptides only in the wild-type (non-treated) (Fig. 2b–f). Exclusively, in the IFN-γ treated samples, a few self-peptides from the TAP1 (AALPAAALW, LLYESPERY, RSLQENIAY, RTALPRIF, SAMPTVRSF, and TEVDEAGSQL) and TAP2 (YLHSQVVSV) were identified (Fig. 2g).

Interestingly, the immunopeptidome data highlights that the majority of MHC-I associated peptides have a length distribution of 9 or 10 mers, and a few peptides around 15-mer in length (Fig. 2d). Particularly, the MHC-I antigen processing involves proteasome-mediated protein degradation as well as TAP-mediated peptide transport, and these processes can generate and handle peptides longer than the canonical 8–10 aa (amino acids) long [91,92]. Stryhn et al. [92] examined the size dependence of peptide binding to MHC-I as well as stimulating T-cells, in proteolytically controlled assay systems by systematically extended the N- and/or C-terminals of optimally sized peptides. Their findings support the consensus view that MHC-I binding and T-cell recognition tends to focus on short well-defined peptides. However, in some cases longer peptides can also bind to MHC-I and such extensions may be accommodated by protrusion out of the MHC-I, and can potentially be recognized by T-cells [92]. In few cases the T-cell can detect the identity of the extension (that it could be part of the specificity of the T-cell immune response) and such extensions may play a physiological role [92]. The crystal structures of peptide bound MHC-I molecules argue in the favor of peptide-size restrictions and suggest that when the anchors are appropriately positioned, slight variations in size can be accommodated through zigzagging or bulging in the middle [92,93]. However, structures involving a protruding C + 1 extension has been determined in which, the C-terminal residue was found to extend up and out of the F-pocket and the corresponding side chains of MHC-I was found to be re-oriented to accommodate

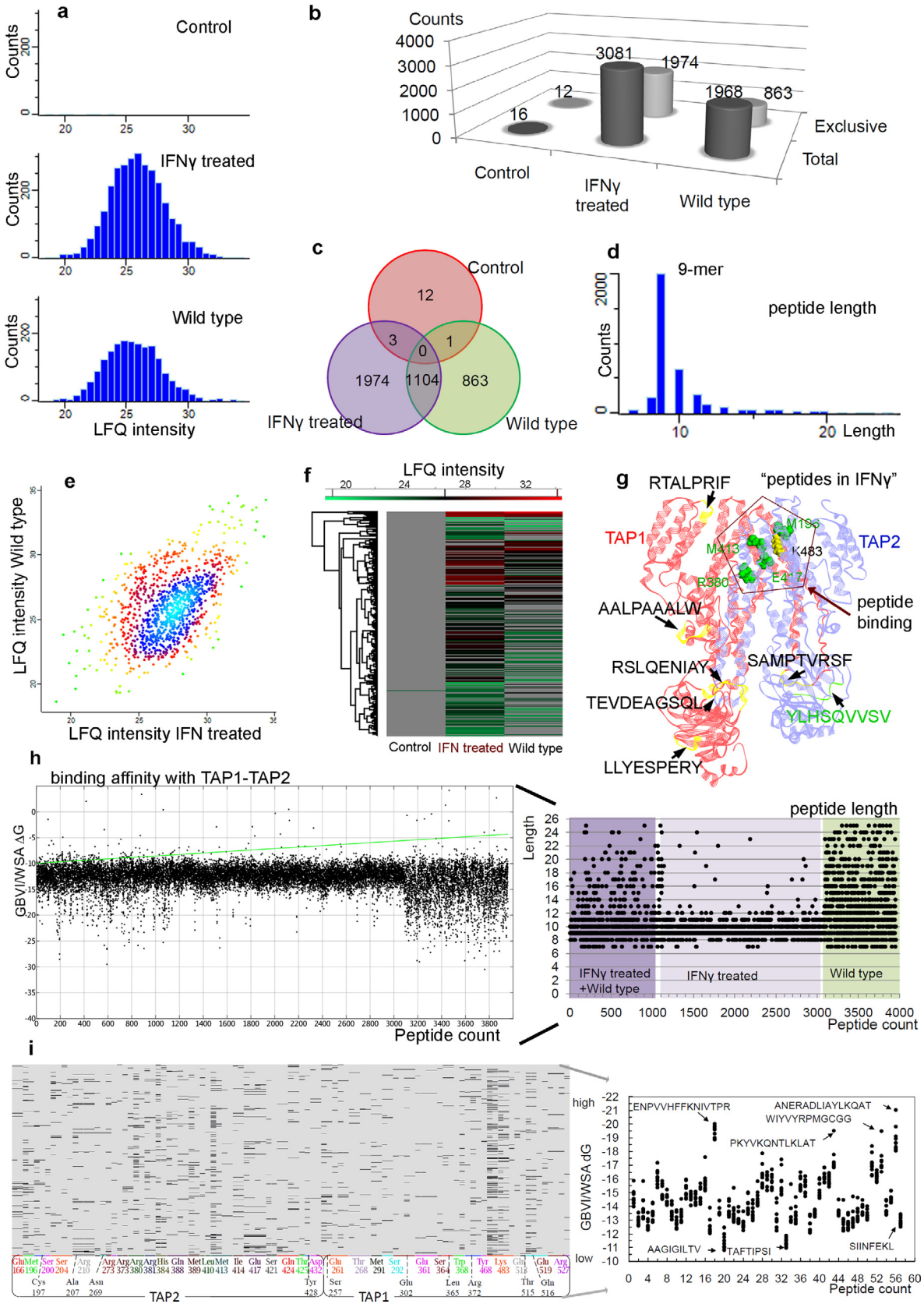
a
Control
IFNγ treated
Wild type
Counts
LFQ intensity
b
Counts
4000
3000
2000
1000
0
16
12
3081
1974
1968
863
Exclusive
Total
Control
IFNγ treated
Wild type
c
Control
IFNγ treated
Wild type
12
3
0
1
1974
1104
863
d
9-mer
peptide length
Counts
Length
e
LFQ intensity Wild type
LFQ intensity IFN treated
f
LFQ intensity
Control
IFN treated
Wild type
g
RTALPRIF
"peptides in IFNγ"
TAP1
TAP2
M413
M196
K483
R380
E417
AALPAAALW
peptide binding
RSLQENIAY
SAMPTVRSF
TEVDEAGSQL
YLHSQVVSV
LLYESPERY
h
binding affinity with TAP1-TAP2
GBVI/WSA ΔG
Peptide count
peptide length
Length
IFNγ treated +Wild type
IFNγ treated
Wild type
Peptide count
i
TAP2
TAP1
high
low
GBVI/WSA dG
ENPVVHFFKNIVTPR
ANERADLIAYLKQAT
WIYVYRPMGCGG
PKYVKQNTLKLAT
AAGIGILTV
TAFTIPSI
SIINFEKL
Peptide count

the peptide extension [92]. This explains the flexibility of the otherwise apparently closed binding cleft of the MHC-I allowing for binding of different peptide sizes as long as the binding energy is sufficient [92]. Moreover, it has been shown that naturally bound peptides eluted off the MHC-I spans a size range from 6 to 33 aa, although the majority (∼80%) were of the canonical 8–11 aa [92,94,95]. The proteasome generates peptides varying in size from 4 to 24 aa, and it has been estimated that ∼30% of the peptides are 8 aa or longer. The TAP transporter can translocate peptides up to 40 residues long, though 8–13 residues long peptides are transported most efficiently [92,96].

In silico virtual screening of peptide datasets was performed against the TAP1-TAP2 transporters and the resultant TAP-peptide complexes were ranked by the docking score (GBVI/WSA dG, kcal/mol; Fig. 2h and i). The MHC-I peptide having the length of 8, 9, or 10 mers shows a binding affinity between −10 to −15 kcal/mol (GBVI/WSA dG; Fig. 2h) with the TAP1-TAP2 transporters. Peptides having a length of 14–26 amino acids formed binding affinities with the TAP transporters in the range of −20 to −25 kcal/mol (GBVI/WSA dG; Fig. 2h). Overall, the peptides identified from the IFN-γ treated samples exhibited less affinity with the TAP proteins, compared to the peptide from the untreated cells. In addition, the binding affinity difference of peptides from IFN-γ treated and untreated samples exhibited a correlation with the length of peptide, i.e. and peptides from IFN-γ treated have short length (peptides 1100–3100 in Fig. 2h and Table S5), whereas peptides from untreated are comparatively longer (peptides 3100–3957 in Fig. 2h and Table S5). Based on the peptide binding affinities with TAP transporters and the higher number of 9–10 mers identified in the immunopeptidome (Fig. 2d and h), it could be proposed that peptides having weak binding affinity with the TAP1-TAP2 transporters could exhibit faster transport from the cytosol to the ER. Moreover, it has previously been reported that TAP transporters can translocate 8–13 residue peptides most efficiently [92,96,97]. The IFN-γ treated cells had a higher number of peptides identified compared to the untreated, suggesting that upon inducing immunity, a majority of shorter length peptides have a lower TAP1-TAP2 binding affinity (Fig. 2d and h). In addition, more residues (M196, R380, M413, and E417) from TAP2 were involved in interacting with the peptide, and fewer peptides were detected from TAP2 itself, whereas the reversed was observed for the TAP1 (only residue K483 binds to the peptide; Fig. 2g). In addition, such peptide interacting TAP residues were also previously reported [15].

To further investigate and validate the protein-peptide findings, a separate peptide datasets from the ATLAS database [48] were retrieved alongside the immunopeptidome dataset from the melanoma cells. For these peptides the structures of each TCR-peptide-MHC complex is known, and we screened them against our modeled TAP1-TAP2 transporters (Fig. 2i, S1, S2, and Table S4). Analysis of the immunopeptidome data and peptides from the ATLAS database [48] (Fig. 2h and 2i) correlated with each other, in terms of binding affinity versus the peptide length (Fig. S3a and S3b). Most peptides with 8 or 9 mers length exhibited lower binding affinity with TAP compared to the longer peptides (Fig. S3c and S3d). TAP1 and TAP2 residues forming the interactions with the studied set of peptides were identified, which highlights an overlap between immunopeptidome peptides and peptides from ATLAS database (Fig. S3a and S3b). Additionally, the binding conformations of a few peptides showing highest and least affinity to TAP were: pep56 (ANERADLIAYLKQAT) −21.03 kcal/mol, pep18 (ENPVVHFFKNIVTPR) −20.02 kcal/mol, pep53 (WIYVYRPMGCGG) −19.49 kcal/mol, pep43 (PKYVKQNTLKLAT) −19.52 kcal/mol, pep57 (SIINFEKL) −13.44 kcal/mol, pep20 (AAGIGILTV) −12.46 kcal/mol, and pep33 (TAFTIPSI) −11.87 kcal/mol. Among which the dynamics of the pep18, pep20, and SIINFEKL (8-mer model) peptides with the TAP1-TAP2 transporters were further analysed (Fig. 2i and S2).

3.2. Scaling effects of viral proteins and somatic mutations on the TAP transporters

The modeled viral protein structures were screened against the predicted active sites, and the data suggests that all selected viral protein inhibitors targeted the peptide transport pockets of TAP proteins through different possible interactions. The binding free energy reports (GBVI/WSA dG; kcal/mol) and binding mode of viral proteins to TAP structure are shown in Fig. 3a. Among different viral proteins screened against the TAP1-TAP2 complex, the ICP47 protein formed the highest affinity (−108.18 kcal/mol), and in the second position is the BNLF2a protein with binding affinity of −90.08 kcal/mol, whereas the proteins CPXV012, US6, and UL49.5 obtained almost similar affinity (−81.71 kcal/mol, −85.27 kcal/mol, and − 85.28 kcal/mol, respectively). The binding mode of viral protein inhibitors to TAP correlates with the proposed models [38]; four out of five viral proteins targeted the helical regions (Fig. 3a) of TAP1 and showed a similar pattern of blocking the peptide translocation cavity of the TAP transporter. The US6 protein binds to both TAP transporters at the loop regions toward the ER lumen, with almost similar affinity (Fig. 3a).

Single nucleotide polymorphisms are one of the most common forms of genetic variation, and a large number of human genes associated with viral infections comprise SNPs [98]. For both TAP1 and TAP2 transporters, the SNPs were identified and to assess the polymorphisms, the residues from TAP transporters involved in binding with the viral proteins (within 8 Å; BNLF2a, CPXV012,

Fig. 2. Comparative immunopeptidome analysis. (a) Logarithmized log2(x) data, after reverse filtering the rows using categorical columns, for the MHC-I peptide presentation from the control, IFN-γ treated, and non-treated (termed as wild-type in this study) samples. (b) Peptide counts per sample, as well as the exclusive MHC-I peptides for a particular sample. (c) Venn diagram representing the common and unique peptides in all three/two respective samples. (d) Length distribution of the MHC-I peptide that were identified in all three samples (control, IFN-γ treated, and untreated/wild-type). (e) and (f) Scatter plot and heat map describing the LFQ intensities between wild-type vs IFN-γ treated samples. (g) TAP1 and TAP2 peptides identified (presented over MHC-I molecule) only in the IFN-γ treated samples, labeled in black (marked yellow) are from TAP1 and in green are from TAP2. (h) Identical 3957 peptides from three samples (control, IFN-γ treated, and non-treated) were screened against the TAP1 and TAP2 transporters. Right panel represents the peptide length (differentiated according to the samples), and the left panel represents particular peptide binding affinity with TAPs (five different conformations per peptide). In panel g; residues K483 (TAP1) and M196, R380, M413, and E417 (TAP2) were found commonly interacting with the 3957 peptides (from control, IFN-γ treated, and non-treated), docked with TAP1 and TAP2 are highlighted (yellow from TAP1 and green from TAP2). (i) Barcodes represent (left panel) fingerprint analysis of peptides (from the ATLAS database [48]) forming interactions with TAP1 and TAP2 proteins (Table S4), and the selected peptide fingerprints as a matrix (one row per entry, one column per fingerprint bit) in which a set bit is drawn as a black rectangle. X-axis shows the residue numbers that correspond to each group of fingerprint bits, and is coded with an arbitrary sequence of colors. The scattered plot (right panel) represents the binding affinity of each peptide against TAP transporters. Peptides with the highest and lowest binding affinity are highlighted, and few were selected for MD simulations in order to examine their kinetics. The plot (right panel) presents a binding affinity of 10 conformations for each peptide against the TAP1-TAP2 transporters. (For interpretation of the references to color in this figure legend, the reader is referred to the web version of this article.)

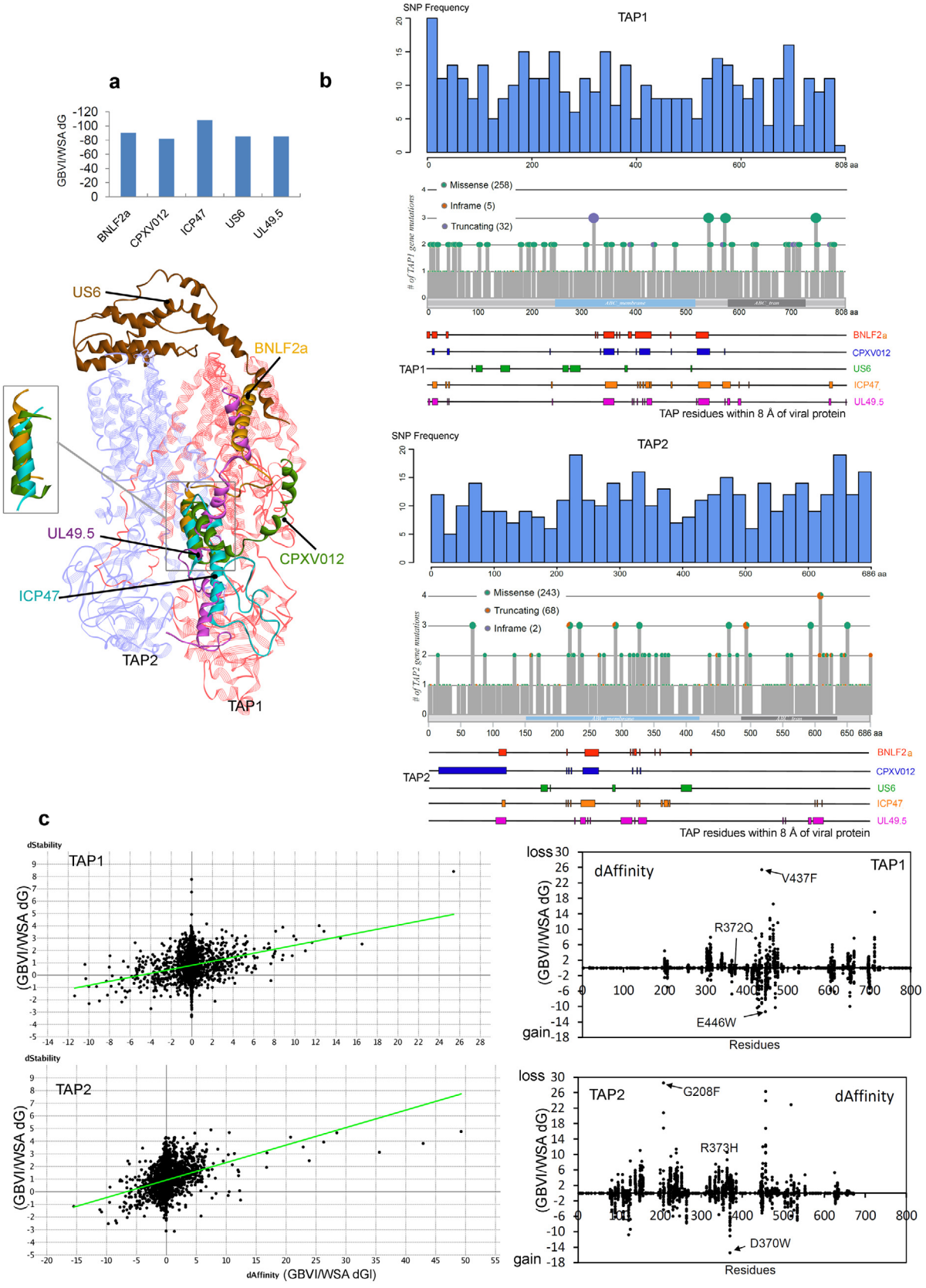
a
GBVI/WSA dG
BNLF2a
CPXV012
ICP47
US6
UL49.5
US6
BNLF2a
UL49.5
CPXV012
ICP47
TAP2
TAP1
b
SNP Frequency
TAP1
Missense (258)
Inframe (5)
Truncating (32)
# of TAP1 gene mutations
BNLF2a
CPXV012
US6
ICP47
UL49.5
TAP1
TAP residues within 8 Å of viral protein
SNP Frequency
TAP2
Missense (243)
Truncating (68)
Inframe (2)
# of TAP2 gene mutations
BNLF2a
CPXV012
US6
ICP47
UL49.5
TAP2
TAP residues within 8 Å of viral protein
c
dStability
TAP1
(GBVI/WSA dG)
dStability
TAP2
(GBVI/WSA dG)
dAffinity (GBVI/WSA dGl)
loss
dAffinity
TAP1
V437F
R372Q
E446W
gain
(GBVI/WSA dG)
Residues
loss
TAP2
G208F
dAffinity
R373H
D370W
gain
(GBVI/WSA dG)
Residues

ICP47, US6, and UL49.5) were traced (Fig. 3b and Tables S6–S7). Overall, both TAP1 and TAP2 transporters behave differently when correlating SNPs to that of the TAP interacting residues with viral proteins. Exclusively for TAP1, the frequency of SNPs was found lower in the regions binding to viral proteins (Fig. 3b). These data suggest that the viruses may aim for the most conservative TAP1 regions (Fig. 3b and Tables S6–S7). On the contrary, for TAP2 the frequency of SNPs was found higher in the regions binding with viral proteins (Fig. 3b). Like the SNPs in the TAP transporters (Fig. 3b), a similar trend was observed in the analysis of cancer-associated mutations in both TAP transporters, i.e. for TAP1 protein regions with less cancer variants were targeted by viruses, whereas in TAP2 highly mutated regions were involved in binding with viral protein (Figs. 1e and 3b).

Mutations in a protein may affect its structural stability, disrupt protein interactions, render proteins non-functional, and potentially promote tumor progression [72]. Therefore, along with the cancer-associated variants from the TAP transporter retrieved from the COSMIC (cancer.sanger.ac.uk) and cBioPortal (www.cbioportal.org), and screened for change in structural stability and binding (TAP1-TAP2) affinity, these hotspots regions or amino acids were also screened by mutated with the other 20 amino acids (Fig. 3c). The findings suggest that point mutations in either TAP1 or TAP2 are sufficient to alter the protein–protein interactions, which can significantly affect the peptide binding or the peptide transport process (Fig. 3c). Screening (fingerprint) analysis indicate that TAP1 or TAP2 peptide interacting interface (Fig. 2i), are also found mutated in different cancer types. Such residue variants are; R372Q, S364R, S364I, Q516K, E519K, and R527K from TAP1 protein, and E166G, E166K, M196V, R210L, R373H, and S200F from TAP2 (Fig. 3c). Considering the peptide binding region [15] and protein–protein interface, cancer mutations and their binding affinity, $TAP1_{R372Q}$ and $TAP2_{R373H}$ were further studied by MD simulations. In addition, the cancer derived mutants inducing highest (best) and lowest binding affinity were selected for MD simulation analysis: $TAP1_{V437I}$ (−7.92 kcal/mol), $TAP1_{V437F}$ (25.43 kcal/mol), $TAP1_{E446K}$ (−5.99 kcal/mol), $TAP1_{E446W}$ (−11.35 kcal/mol), $TAP2_{D370N}$ (−1.23 kcal/mol), $TAP2_{D370W}$ (−15.43 kcal/mol), $TAP2_{G208S}$ (1.62 kcal/mol), and $TAP2_{G208F}$ (28.53 kcal/mol; Fig. 3c).

3.3. Viral components with similar modulatory actions towards the TAP transporters

Viral proteins (for example; BNLF2a, CPXV012, ICP47, US6, and UL49.5) can significantly manipulate the peptide transport process by binding directly with the TAP1 or TAP2 transporters. Therefore, to understand the molecular recognition of the TAP1-Virus-TAP2, and particular the different viral proteins (BNLF2a, CPXV012, ICP47, US6, and UL49.5) we simulated their interactions with the TAP transporters (Fig. 4a, represents TAP1-ICP47-TAP2 complex). Evaluating the stability for simulated systems solving the RMSD (root-mean-square deviation of all non-hydrogen atoms) equation, suggests that the majority of the viral protein predominantly destabilizes TAP1 (Fig. 4b), compared to that of TAP2 alone. Particularly, for TAP1 such a visible difference was detected for UL49.5 and BNLF2a, whereas for TAP2 the UL49.5 induced the highest fluctuation and BNLF2a the least (Fig. 4b). The apo-form of TAP1 showed a persistent RMSD plot (∼8 Å) during the 100 ns of MD simulations, whereas the TAP2 showed a slightly increasing flexibility over time that stabilized between ∼70–100 ns (Fig. 4b). The RMSD findings suggest that the UL49.5 exhibited the highest fluctuations and BNLF2a was the most stable of the viral proteins (Fig. 4b).

Moreover, solving the RMSF (root mean square fluctuation) equation over Cα atoms of each amino acid revealed a similar nature for both TAP transporters, i.e., a majority of residues in the apo-system were more stabile as compared to the viral-bound systems, except for some residues in TAP2 (for example 390–410 aa; Fig. 4c). Such behavior of TAP2 residues from RMSF correlated with the RMSD data which showed a slightly increasing flexibility of TAP2 over time (Fig. 4b). The dynamics of the TAP1/2-viral protein complex dynamics suggest that upon binding of the viral proteins, an allosteric effect inducing increased amino acid fluctuations in several regions of both transporters were indicated (Fig. 4c). Interestingly, the TAP1 peptides (97RTALPRIF104, 206AALPAAALW214, 432SAMPTVRSF440, 653RSLQENIAY661, 694TEVDEAGSQL703, and 744LLYESPERY752) and TAP2 peptide (541YLHSQVVSV549) presented on the MHC-I molecules upon IFN-γ treated melanoma cells (Fig. 2a), originates from the highly fluctuating regions directly interacting with viral factors or allosterically affected by viral binding (Fig. 4c).

The structural dynamics of the TAP1-TAP2 complex in the presence and absence of a viral proteins revealed that, in all simulated systems the TAP_{NBD} domains formed a tilt movement toward the cytosol membrane (Fig. 4d and Videos S1, S2). Such displacement of the TAP_{NBD} domains creates a passage in the transport channel formed by TAP1 (helix_4; 501–544, helix_5; 338–376, helix_6; 384–425) and TAP2 (helix_5; 249–289, helix_6; 294–344); opened towards cytosol (Fig. 4d). From these data it may be proposed that the opening or closing of the cytosolic passage by the TAP transporters (TAP_{NBD} domains) can be associated with ATP hydrolysis, and thus, resulting in the peptides being directly presented to the PLC complex. This cytosolic "open-state" transport channel of the TAP proteins, may intake peptides from cytosol-towards-ER and was targeted by 4 (BNLF2a, CPXV012, ICP47, and UL49.5) out of 5 studied viral proteins blocking the transport channel (Figs. 4d and S4).

Viral proteins have increased the protein–protein intermolecular interactions between TAP transporters compared to that of the apo-system (Fig. 4e and Table S8). A slight difference is observed concerning the viral proteins when interacting with TAP1 or TAP2, i.e., BNLF2a, CPXV012, and ICP47 formed a higher number of interactions with TAP1, whereas UL49.5 and US6 shared relatively equal interactions with both transporters (Fig. 4f). These

Fig. 3. *In silico* screening of viral proteins, peptides, and cancer-associated mutations on the TAP1-TAP2 transporters. (a) Viral proteins (BNLF2a, CPXV012, ICP47, US6, and UL49.5) docked with the TAP transporters, and the binding conformations for each studied viral components resembles almost a complementary state (Fig. 1b), as well as proposed in different studies [18,23,38]. In addition, 4 out of 5 viral proteins assembled a similar conformational pattern to block the peptide transportation cavity in TAP proteins. (b) Lollipop plots for the TAP1 and TAP2 gene mutations, colours in the figure represent different types of polymorphism. In the top panel of each lollipop plot, a bar plot represents the cumulative frequency of mutations for each 20 amino acids. On the bottom panel, the regions of interaction from the TAP1 and TAP2 proteins with the viral proteins are represented in different colours (identified in virtual screening; Fig. 3a). (c) Mutational landscape of TAP1 and TAP2 proteins, datasets of cancer variants from COSMIC (cancer.sanger.ac.uk) and cBioPortal (www.cbioportal.org) were screened with the TAP transporters tracing their change in stability (GBVI/WSA dG, kcal/mol) and affinity (GBVI/WSA dG, kcal/mol) upon mutation (applying residue scan methodology in MOE [68]). In addition to the cancer-associated mutations from COSMIC (cancer.sanger.ac.uk) and cBioPortal (www.cbioportal.org), each amino acid was mutated with other 20 amino acids [A, R, N, D, C, Q, E, G, H, I, L, K, M, F, P, S, T, W, Y, and V] to search for mutations that change the binding affinity (GBVI/WSA dG, kcal/mol). The left panel describes a comparison of change in structural stability with change in binding (TAP1-TAP2) affinity upon introducing each amino acid variant. The right panel scatter plot describes the effects of mutant residues (from TAP1 or TAP2) on the protein–protein binding affinity (GBVI/WSA dG, kcal/mol).

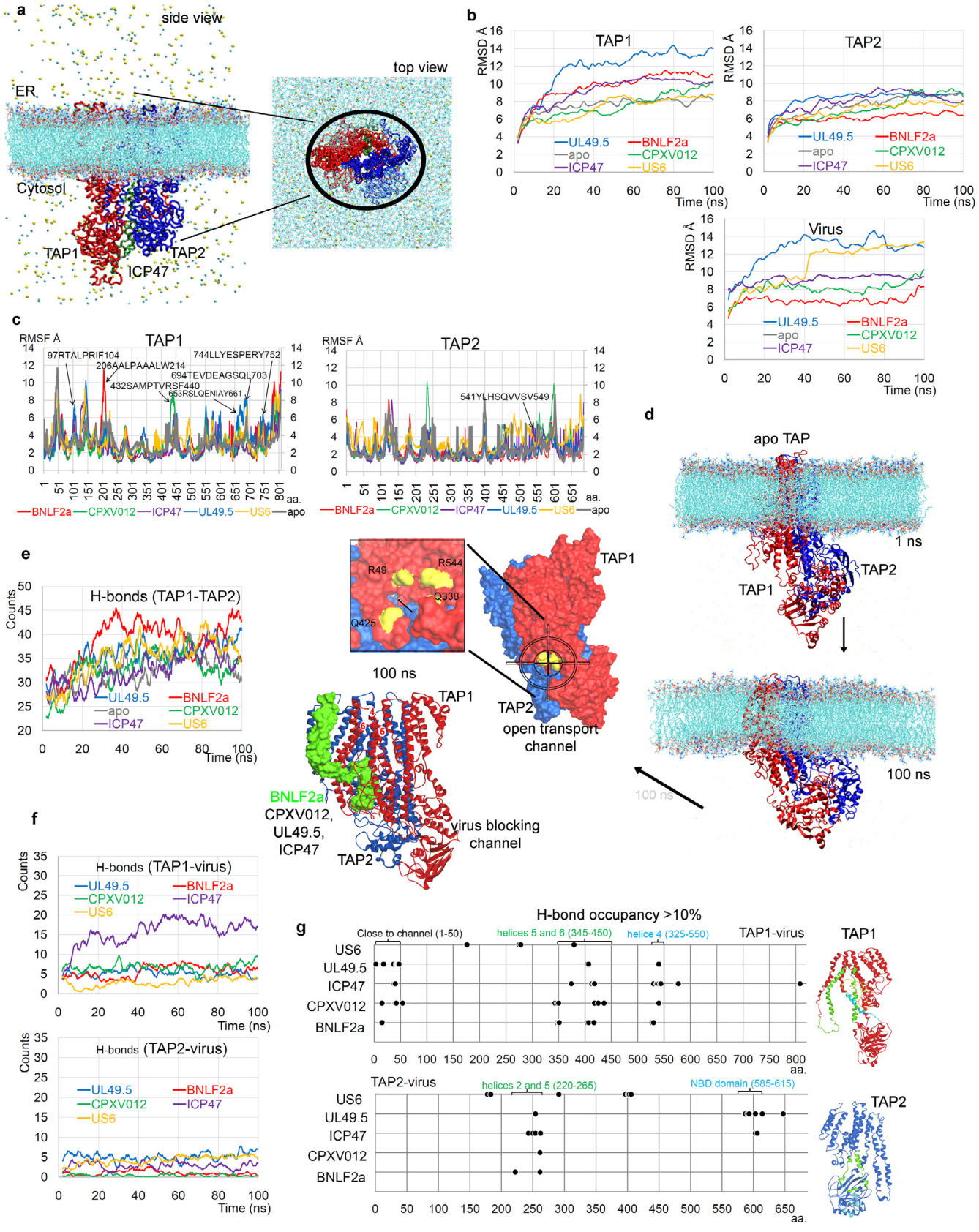
a
side view
top view
ER
Cytosol
TAP1
TAP2
ICP47
b
TAP1
TAP2
Virus
RMSD Å
Time (ns)
UL49.5
BNLF2a
apo
CPXV012
ICP47
US6
c
RMSF Å
TAP1
TAP2
97RTALPRIF104
206AALPAAALW214
432SAMPTVRSF440
663RSLQENIAY661
744LLYESPERY752
694TEVDEAGSQL703
541YLHSQVVSV549
aa.
BNLF2a CPXV012 ICP47 UL49.5 US6 apo
d
apo TAP
1 ns
TAP1
TAP2
100 ns
e
H-bonds (TAP1-TAP2)
Counts
Time (ns)
R49
R544
Q338
Q425
TAP1
TAP2
open transport channel
100 ns
BNLF2a
CPXV012,
UL49.5,
ICP47
virus blocking channel
f
H-bonds (TAP1-virus)
H-bonds (TAP2-virus)
g
H-bond occupancy >10%
Close to channel (1-50)
helices 5 and 6 (345-450)
helice 4 (325-550)
TAP1-virus
TAP2-virus
helices 2 and 5 (220-265)
NBD domain (585-615)
aa.

intermolecular transporter-viral interactions (Fig. 4f) together with the SNPs data and cancer mutations (Figs. 1 and 3), suggest that in the case of TAP1 protein regions with lower SNPs frequency as well as a few cancer variants was found making higher interactions with viral factors. On the contrary viral factors binds highly mutated TAP2 regions. Long lasting interactions ≥10 ns between TAP-viral proteins were identified and are presented in Table S9. Particularly, a higher number of residues from TAP1 were involved in the interactions with viral components, compared to the TAP2 gene (Table S9). TAP1 amino acids from helices 4, 5, and 6 (residues range 345–450 aa and 325–550 aa), as well as from residue range 1–50 aa located close to the transport channel were found to interact with viral factors (Fig. 4g and Table S9). Additionally, the TAP2 residues in range 220–265 aa (from helices 2 and 5) and 585–615 aa (TAP_{NBD} domain) were involved in binding viral proteins (Fig. 4g and Table S9). Several amino acids from TAP1 or TAP2 were found in common when interacting with BNLF2a/CPXV012/ICP47/UL49.5 viral factors. Exceptionally, the US6 protein have a unique interacting residues from the transporters that were not identified in other studied TAP-virus complexes (Fig. S4b). For the TAP1 protein, residue E540 was found interacting with three different viral proteins (UL49.5, ICP47, and CPXV012), and residues D15/R347/E350 and R40/E418/E536 were found common binding with BNLF2a/CPXV012 and ICP47/ CPXV012, respectively. From the TAP2 transporter, residues S254 and K603 were involved in binding with the ICP47 and UL49.5 viral factors (Fig. S4b).

3.4. Distinctive behavior by TAP transporters to drive short vs long peptide antigens towards the ER lumen

To understand the kinetics or movements of the peptides through TAP transport tunnel, the MD simulations were performed for three different peptides that vary in lengths; pep18 (15 aa), pep20 (9 aa), and SIINFEKL (8 aa). The deviation and fluctuation plots (Fig. S5) explain that all systems have reached their stability, and in particular, TAP1 showed more flexibility in complex with longer peptide; pep18 (Fig. S5a). Individual amino acid fluctuations for the TAP proteins suggest that the presence of shorter peptides (pep20 and SIINFEKL) induced stability in the transporter, compared to pep18 peptide (15-mer; Fig. S5b). Moreover, the self-peptides of TAP1 and TAP2 identified in the immunopeptidome data (Fig. 2) were highly flexible region in viral bound systems (Fig. 4b), the majority of these regions lacked such fluctuation differences in the peptide-bound systems (Fig. S5a).

The structural movements of the TAP transporters towards the ER lumen, suggests that the TAP transporters can have two separate cytosol-to-ER peptide passages (Fig. 5a and b). Fig. 5b, represents four helices from each TAP protein that can be involved in the placing of the peptides toward the ER lumen, and to measure the opening or closing of the transportation cavity the area based on the Cα (C-alpha) atoms from the respective helices were identified; area 1 (TAP1; S496 and S501, TAP2p; D185) and area 2 (TAP1; ASP278, TAP2; S393 and S408) (Figs. 5b, 6, and 7). Particularly, for the SIINFEKL (8-mer) that is smaller in length compared to the pep18 (15-mer), only the passage formed by two helices from each TAP1 and TAP2 was found open. Passage 1 or area 1 is in the closed conformation, whereas area 2 is in the open state that could allow the SIINFEKL peptide to be transported. In the presence of pep20 (9-mer), a moderate opening as well as closing state of the transport passage was observed, i.e., during the first 25 ns only area 2 formed an open-state conformation, whereas at the end of MD simulation (∼85–100 ns), only area 1 formed an open-state (Fig. 5a and b). However, the pep20 system comparatively had less differences between both areas as that of the SIINFEKL system. This could be a consequence of a different sequence composition of peptides that can have different interactions with TAP transporters. For the system with pep18, both passages formed by 8 helices (4 from each TAP1 and TAP2) are in the open state. These differences in conformations by TAP correlates well with the areas computed as shown in Fig. 5a, i.e., area 1 for systems with SIINFEKL peptide reaches upto 250 $Å^2$ and area 2 is mainly limited to 90 $Å^2$. On the contrary, with pep18, both area 1 and area 2 are found in the open state, which ranges from ∼110–300 $Å^2$ (Fig. 5a). Overall, based on the areas computed on TAP transporter towards ER-opening, a difference in the transport of longer vs shorter peptides was identified. However, the sequence composition of the peptide can also affect the rate of such conformation by the transporters (Fig. 5a and b).

Additionally, there are efforts made to understand the mode of substrate translocation and transports by different ABC exporters, and the most common proposed/suggested is the IF-to-OF (inward- to outward-facing) conformational transition/switch [99–102]. Particularly, the IF-to-OF switch has been confirmed by the cryo-electron microscopy (cryo-EM) [100] for the heterodimeric TmrAB (Thermus thermophilus multidrug resistance proteins A and B); a TAP structural homolog which also can restore antigen processing in human TAP-deficient cells [100,102]. In the TmrAB transporters during the inward-facing (IF state; TmrAB allows binding of nucleotides and peptide, which has a closed state at the top) conformations of the NBD domain can obtain a wide distance and in the outward-facing (OF state; abolished peptide binding and nucleotide exchange, which opens in the top) the conformation the NBD domains is represented in a close contact. Hence, to analyze such conformational switch movements by the NBD domains ($TAP1_{NBD}$ 550–808 aa and $TAP2_{NBD}$ 450–686 aa) from the TAP1 and TAP2 heterodimer, we measured the distance centre of mass between NBD domains from both TAP transporters in the presence or absence of the peptide. The dynamic behavior of the apo-systems; wild-type (Fig. 4d) and mutated (Fig. 4c), have shown a closed conformation towards the ER lumen (IF conformation; NBD has wide distance), whereas in the presence of peptide the transport channel is found in the open state towards the ER lumen (OF conformation, NBD has close contact; Fig. S6). The distance between NBD domains in the wild-type apo-system remained higher (∼42.31 Å) throughout the MD simulations (Fig. S6), whereas in the presence of peptide the distance dropped to 34.03 Å from 42.31 Å. These findings correlate with the area computed for the transport channel (Fig. 5a), that when the channel

Fig. 4. The binding interfaces of different viral proteins (BNLF2a, CPXV012, ICP47, US6, and UL49.5) with the TAP1-TAP2 transporters. (a) One molecular dynamic cell in periodic boundary conditions (for example, the TAP1-ICP47-TAP2 complex), which includes proteins, water, and ions. (b) RMSDs of the TAP transporters from the MD simulations, and the bottom panel describes the RMSDs of viral factors. (c) RMSFs of individual amino acids from both TAP transporters. (d) Structural dynamics of the TAP1-TAP2 transporters representing the tilt movement of the $TAP1/2_{NBD}$ domains forming an entry gate or transport channel open toward the cytosol. In addition, the majority of the studied viral proteins in this work were found interacting with the passage or open transport channel which could block the peptide from invading the transport channel. TAP1 helices (helix_4; 501–544 aa, helix_5; 338–376 aa, helix_6; 384–425 aa) forming an open cytosolic passage and binding with the viral proteins are labeled. (e) The intermolecular hydrogen bond interactions formed between the TAP1 and TAP2 proteins during the MD simulation time course and with occupancy ≥10%, in the presence and absence of different viral proteins. (f) Hydrogen bond interactions between the viral protein and the TAP transporters. (g) Residues from TAP1 or TAP2 involved in binding viral proteins with occupancy ≥10%, and the right panel represents the position of these regions over the protein structure.

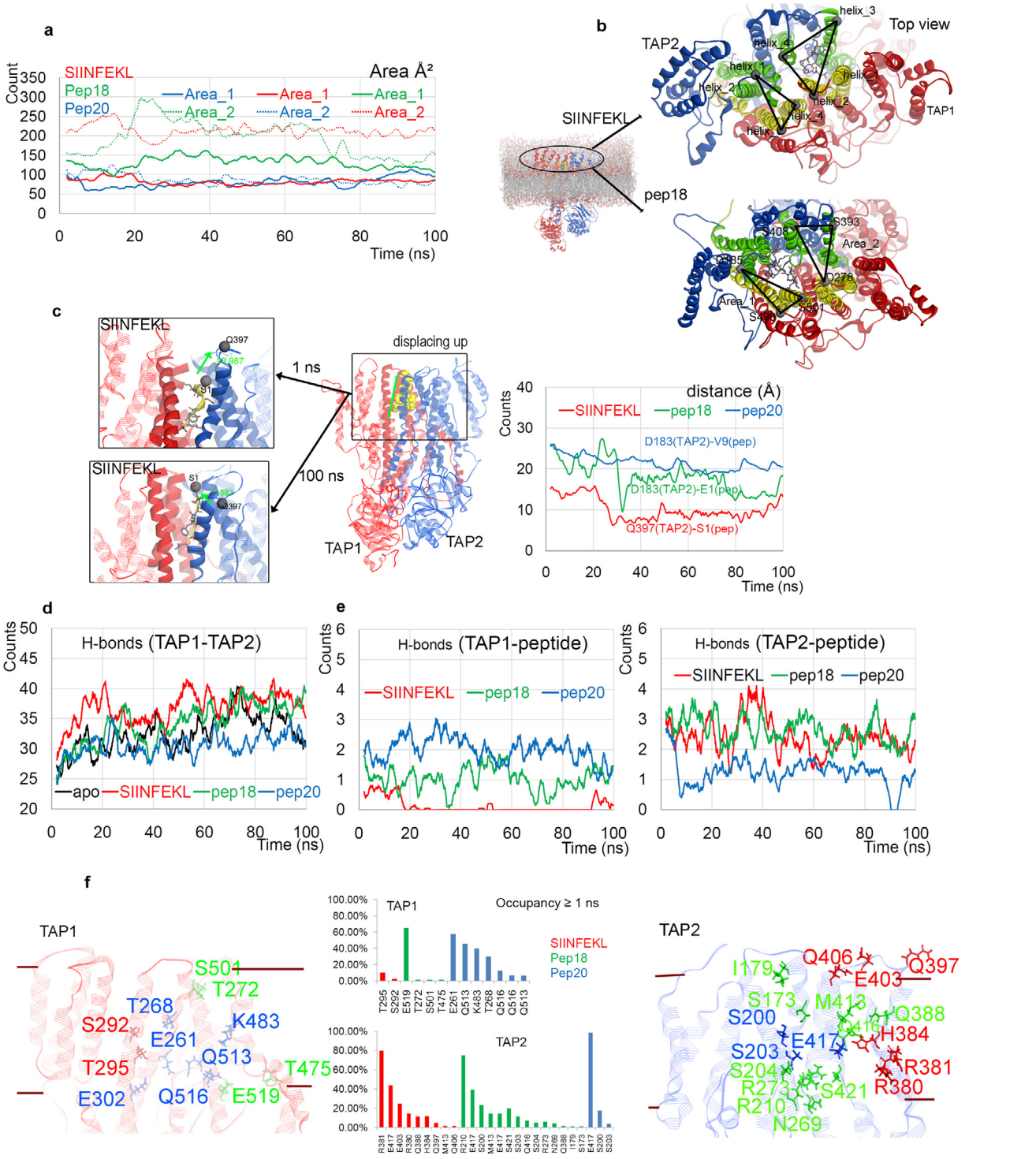

Fig. 5. The binding interface with dynamics of the pep18, pep20, and SIINFEKL peptides with TAP transporters. (a) and (b) Area computed considering the four helices each from TAP1 or TAP2 involved in forming the passage for the transportation of the peptide, as represented in b. C-alpha (CA or Cα) atoms coordinates of each residue were traced over time evaluation of the molecular dynamics; area 1 = TAP1 (SER496 and SER501) and TAP2 (ASP185) and area 2 = TAP1 (ASP278) and TAP2 (SER393 and SER408). Helices residues range; TAP1 = 256–275 aa (helix_1), 281–329 aa (helix_2), 451–495 aa (helix_3), 501–544 aa (helix_4), and TAP2 = 145–181 aa (helix_1), 189–226 aa (helix_2), 356–395 aa (helix_3), and 405–440 aa (helix_4). (c) The displacement of the peptides from the centre of the transportation cavity towards the ER lumen. In addition, to measure the movements of peptides in the transport tunnel, distance between the TAP2 (from top, toward ER lumen) and peptide Cα atoms were computed for the selected amino acids; Q397(TAP2)-S1(SIINFEKL), D183(TAP2)-E1(pep18), and D183(TAP2)-V9(pep20). (d) and (e) Intermolecular hydrogen bond interactions between the TAP1 and TAP2 (protein–protein), and TAP1/TAP2-peptide, respectively. (f) TAP residues involved in forming hydrogen bond interactions with pep18, pep20, and SIINFEKL peptides with an occupancy of ≥1%.

opens towards the ER lumen, the NBD domain forms a closed conformation (Fig. S6), as observed in the IF-to-OF conformational switch for other ABC transporters [99–102].

To understand the kinetics of the peptide inside the TAP cavity, the distance between the TAP residue from the top or surface open towards the ER lumen and the residue from the peptide heading

upwards in the cavity was traced (Fig. 5c). The distance between Q397(TAP2)-S1(SIINFEKL) dropped from 15 Å to 5 Å (Video S3), suggesting a peptide upward displacement mechanism. A similar trend in the drop of distance between TAP amino acids from top and from the peptide residue was observed for pep18 and pep20 (Fig. 5c and Video S4). Comparing the drop down of distances with each peptide, it was observed that a shorter peptide (SIINFEKL) has initiated movements relatively earlier compared to the longer peptide (pep18; Fig. 5c). Considering the conformational dynamics and visualizing such distance movement by the peptide in the channel, it is suggested that the actual movement is coming from the peptides (Fig. 5c).

Hydrogen bonds between TAP1-TAP2 in the presence of the peptide (Fig. 5d), suggest that a higher number of interactions occur when there is an increase in the movement (opening of the cavity as shown in Fig. 5a and b). Particularly, the system with the SIINFEKL and pep18 peptides obtained more protein–protein interactions compared to that of the apo-form and pep20 system (Fig. 5d). In addition, higher numbers of arginine-glutamic acid residue pairs were observed forming the TAP1-TAP2 interaction interface (Table S10). Furthermore, the interactions between the peptides and TAP1/2, suggests that SIINFEKL and pep18 obtained few interactions with TAP1 but more interactions with TAP2, whereas the opposite behavior was observed for pep20 (Fig. 5e). These findings demonstrate that when the TAP1-TAP2 cavity is in its open conformation towards the ER lumen and the SIINFEKL peptide reaches the top of the TAP transport channel (as shown in Fig. 5c), peptide mostly interact with TAP2 (Fig. 5e). It can also be proposed that TAP1 can be responsible for pulling the peptide from the cytosol and positioning it in the TAP cavity. For each peptide systems (pep18/pep20/SIINFEKL) different amino acids from TAP1 were involved in binding with peptides, and a similar behavior was observed for TAP2 but with some exceptions (Fig. 5f and Table S11). The S203, Q388, and M413 amino acids from the TAP2 proteins were found to be involved in common in at least two peptide systems (Fig. 5f and Table S11). The review by Elisa et al. [8] described a 3D homology model of the human TAP complex based on TmrAB along with essential residues necessary for the antigen processing by TAP [8,103]. Comparing such residues with our peptides screened against the TAP transporters and molecular dynamics data (occupancy > 1 ns), suggest several common residues traced by Elisa et al. [8,103]. Particularly, the TAP1 E519 and TAP2 R380 residues form high occupancy interactions 65.03% and 14.59% (Table S11) with the peptides, respectively. Additionally, TAP1 residues T475, K483, S501, Q513, Q516, and E519 (Table S11) form high occupancy interactions with the studied peptides residing into the peptide binding regions P435-M480 and Q513-R547 determined by mutation studies [8,103]. Similarly, the TAP2 residues R380, R381, H384, Q388, M413, Q416, E417, and S421 (Table S11) show stable high occupancy interactions with the studied peptides, and belongs to the peptide binding region R354-M389 and I414-M433 determined by mutagenesis [8,43,103]. Moreover, here we would like to highlight that during our screening of peptides to the TAP complex, the peptide binding cleft was selected for screening (Fig. 2g and S2), and therefore, higher number of residues that were identified from MD simulation data associate to the peptide binding regions [8,43,103].The electron paramagnetic resonance (EPR) studies have shown a conserved distance of ~2.5 nm or ~25 Å between the N and C terminus of the peptides bound with TAP proteins [8,43]. Hence, to trace such behavior of peptides varying in length studied by MD simulations, we measured the distance based on the Cα atoms (Fig. S7a) of N and C terminus residues of the peptides; pep57 (SIINFEKL), pep18 (ENPVVHFFKNIVTPR), and pep20 (AAGIGILTV). All three studied peptides have a similar N and C terminus distance at a particular time step, similar to EPR studies [8,43]. Particularly, the 15-mer (pep18) peptide has a maximum distance of 37.38 Å, the 9-mer peptide (pep20) has the highest distance of 21.57 Å, and the 8-mer peptide (SIINFEKL) has 21.92 Å distance (Fig. S7a). Furthermore, during the 100 ns MD simulation the average distance for the SIINFEKL peptide termini was 19 Å, pep18 was 32 Å, and pep20 was 14 Å. Comparing these N and C terminus distances with the movements of the peptide towards the ER lumen in the TAP binding cavity during simulations (Fig. 5c), it was observed that pep20 has comparatively slower movements as that of other two peptides (SIINFEKL and pep18), and higher number of interactions with TAP1 compared to TAP2 (Fig. 5c). These observations may suggest that the conformation of the peptides can influence the distance and the movement / kinetics of the peptides within the transporter cavity, and from the structural aspects these conformations may vary based on the peptide sequences. The crystal structure of the SIINFEKL peptide with MHC-I is available (pdb id.: 3p9l [104]), as well as for the peptides pep18 (pdb id.: 3pl6 [105]) and pep20 (pdb id.: 3qdj [106]) complexed with the MHC-1 and TCR receptors (Fig. S7b). Therefore, we computed the distance between N and C terminus of peptides when presented to MHC-I molecules, which correlates with the highest distance observed for each peptide during MD simulations (Fig. S7a).

3.5. Cancer-associated variants affecting protein–protein interface, as well as peptide transportation

Single cancer-associated point mutations can significantly affect the heterodimer formation of the TAP transporters as well as the peptide transport process, and thus, to elucidate such mechanism, MD simulations were performed for the selected mutations in TAP showing high versus low binding affinity (Fig. 3c). The cancer-associated variants at positions 446/437 and 208/370 (located at the protein–protein interface; Fig. 6a right panel) in the TAP1 and TAP2 proteins, respectively, produce a distinctive binding affinity between TAP1-TAP2 complexes ($TAP1_{E446K}$, −5.99 kcal/-mol; $TAP1_{E446W}$, −11.35 kcal/mol; $TAP1_{V437F}$, 25.43 kcal/mol; $TAP1_{V437I}$, −7.92 kcal/mol; $TAP2_{D370N}$, −1.23 kcal/mol; $TAP2_{D370W}$, −15.43 kcal/mol; $TAP2_{G208F}$, 28.53 kcal/mol, and $TAP2_{G208S}$, 1.62 kcal/mol; Fig. 3c). In addition, the mutant $TAP1_{R372Q}$ and $TAP2_{R373H}$ were also considered for MD similations, because of its placement at the region where the peptide binds (Fig. 6a right panel). These mutations were studied in the presence or absence of two different peptides (pep18 and SIINFEKL). Particularly, cancer-associated variants $TAP1_{R372Q}$ (found in cervical squamous cell carcinoma, colon adenocarcinoma, glioblastoma multiforme, and cervical squamous cell carcinoma), $TAP2_{R373H}$ (prostate adenocarcinoma and glioblastoma multiforme), and $TAP2_{D370N}$ (found in skin cancer, non-melanoma) are positioned in the peptide binding region (Fig. S8). Additionally, in this position the cancer variant $TAP1_{I333V}$ (found in B-Lymphoblastic Leukemia/Lymphoma and Acute myelomonocytic leukemia (cBioPortal, http://cbioportal.org)), is well studied in terms of its involvement in cancer [49,50]. Since these cancer-associated mutations (Fig. 6a and S9a) maybe involved in the TAP suppression mechanism and reducing MHC-I cell surface, a set of 14 mutated TAP1-TAP2 systems were constructed for MD simulations in the presence or absence of peptides (Figs. 6 and 7).

Except the $TAP1_{V437I}$ all other variants ($TAP1_{E446K}$, $TAP1_{E446W}$, $TAP1_{V437F}$, and $TAP1_{R372Q}$) have induced flexibility in the TAP1 transporter (Fig. 6a, S9, and S10). Upon mutation in TAP1, the complexed TAP2 protein showed a stable behaviour in all mutated constructs (Fig. 6a and S9a). On the contrary, the majority of cancer-associated mutations in TAP2 ($TAP2_{D370N}$, $TAP2_{D370W}$, $TAP2_{G208S}$, and $TAP2_{R373H}$) have induced stability in the TAP2 protein; excluding the $TAP2_{G208F}$ (Fig. 6a, S9a, and S10b). In addition, the TAP1 protein only showed higher flexibility when complexed $TAP2_{G208F}$

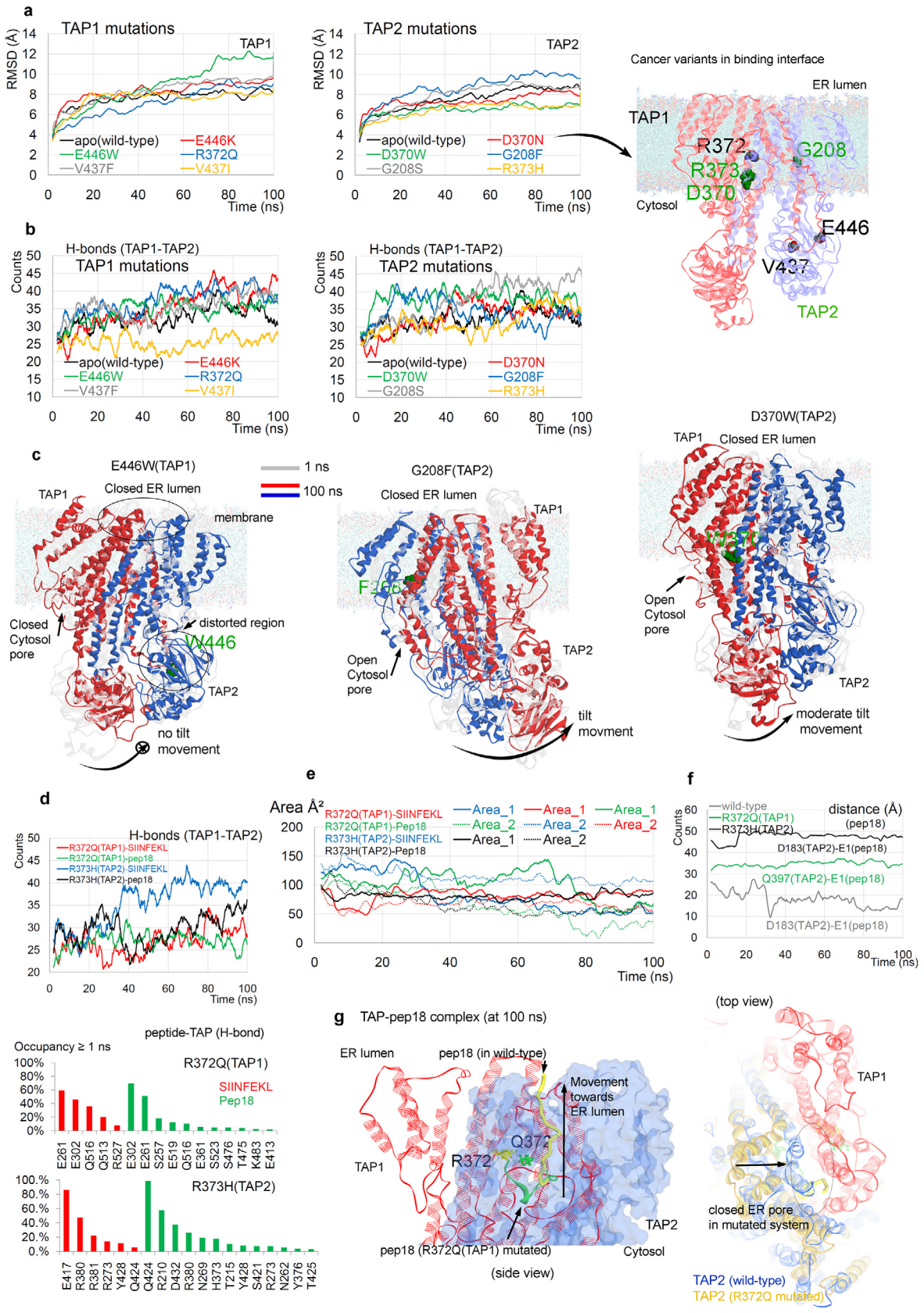
a
TAP1 mutations
TAP1
RMSD (Å)
apo(wild-type)
E446K
E446W
R372Q
V437F
V437I
Time (ns)
TAP2 mutations
TAP2
D370N
D370W
G208F
G208S
R373H
Cancer variants in binding interface
ER lumen
TAP1
R372
G208
R373
D370
Cytosol
E446
V437
TAP2
b
H-bonds (TAP1-TAP2)
Counts
c
E446W(TAP1)
1 ns
100 ns
Closed ER lumen
membrane
Closed Cytosol pore
distorted region
W446
no tilt movement
G208F(TAP2)
F266
Open Cytosol pore
tilt movment
D370W(TAP2)
V437
moderate tilt movement
d
R372Q(TAP1)-SIINFEKL
R372Q(TAP1)-pep18
R373H(TAP2)-SIINFEKL
R373H(TAP2)-pep18
e
Area Å²
Area_1
Area_2
f
wild-type
R372Q(TAP1)
R373H(TAP2)
distance (Å)
(pep18)
D183(TAP2)-E1(pep18)
Q397(TAP2)-E1(pep18)
peptide-TAP (H-bond)
Occupancy ≥ 1 ns
R372Q(TAP1)
SIINFEKL
Pep18
R373H(TAP2)
g
TAP-pep18 complex (at 100 ns)
ER lumen
pep18 (in wild-type)
Movement towards ER lumen
Q372
R372
pep18 (R372Q(TAP1) mutated)
(side view)
(top view)
closed ER pore in mutated system
TAP2 (wild-type)
TAP2 (R372Q mutated)

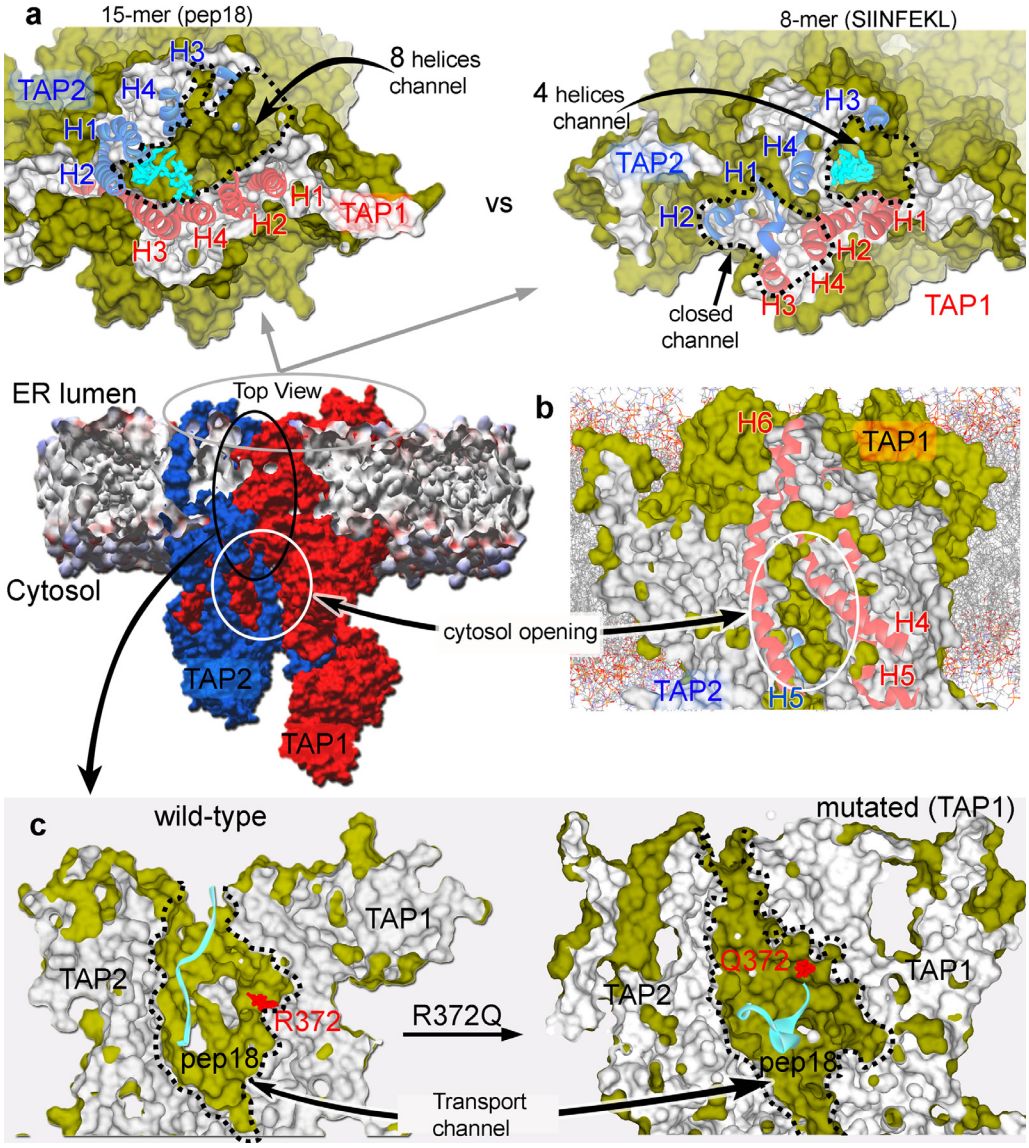

Fig. 7. Structural rearrangements of TAP1-TAP2 transporters examined in the presence of peptide or cancer-associated variants. The protein structures retrieved from the end of MD simulations are represented as surface and slab view, and therefore, the internal regions are in silver color and the surface regions are in dark green. (a) TAP transporters adopted different conformations to transport peptides from cytosol-to-ER, based on the peptide length (for example; 15-mer, ENPVVHFFKNIVTPR, pep18; and 8-mer, SIINFEKL). For a 15-mer peptide, TAP has a 8-helices (four helices from each TAP) transport channel, whereas for an 8-mer peptide, it has a 4-helices (two helices from each TAP) transport channel. Helices are numbered according to Fig. 5b. (b) Cytosolic facing passage in an 'open state' observed during MDS, formed by helix_4 (501–544 aa), helix_5 (332–376 aa), helix_6 (384–425 aa) from TAP1 and helix_5 (250–288 aa) from TAP2. Alone, helix_4 from TAP1 is involved in ER opening as well as cytosolic opening. (c) Mutation in the TAP transport channel (shown in green) can block the peptide in the cavity, for example, $TAP1_{R372Q}$ hinders peptide movement towards ER. *Color Scheme;* TAP1 in red, TAP2 in blue, and peptide in cyan. (For interpretation of the references to color in this figure legend, the reader is referred to the web version of this article.)

(Fig. 6a and S9a). These findings suggest that cancer-associated variants affect both TAP transporters with significantly different effects (Fig. 6a). Furthermore, RMSDs of individual mutated residues at the protein–protein interface suggest that similar as found in initial screen (Fig. 3c) both variants $TAP1_{E446K/W}$ and $TAP1_{V437F/I}$ have contrary behavior, and complementarity was observed for $TAP2_{D370N/W}$ and $TAP2_{G208F/S}$ (Fig. S9b). Interestingly, the variants located at the peptide binding pocket of the TAP1-TAP2 complex

Fig. 6. Mutations affecting the protein–protein interfaces of the TAP transporters, as well as the transport of the peptides. (a) RMSDs of the TAP transporters in the presence of the cancer-associated mutations, and the right panel of the protein structure represents positions of cancer-associated mutations on the protein–protein interface. (b) Intermolecular protein–protein hydrogen bonds between TAP transporters in presence of the cancer-associated variants. (c) Conformation dynamics of the TAP proteins from different mutated systems, representing distinct conformational states upon point mutation. The protein structures were retrieved from the beginning and end of the MD simulations. (d) Intermolecular hydrogen bond interactions between TAP transporters, and the bottom panel represents binding residues of TAP with SIINFEKL or pep18 peptides in the presence of mutations. (e) Area computed for four helices forming the passage for the transportation of the peptide, as represented in Fig. 5b. (f) Distance between the peptide residue and the TAP2 (from top) residue facing from the ER lumen. (g) Conformation dynamics with comparison of the mutated and wild-type system, showing the mutated variants induce rigidity and hinder the transportation of the peptide from cytosol to the ER lumen. Protein coordinates were extracted from the end of the MD simulations.

have diverse conformations; the $TAP1_{R372Q}$ variant was found highly stable, whereas the $TAP2_{R373H}$ showed a paradoxical data (Fig. S9b).

Increasing flexibility in TAP1 in the mutated form (in the absence of peptide), induced a higher number of intermolecular protein–protein (hydrogen bonds; H-bonds) interactions compared to that of the wild-type system, except for the $TAP1_{V437F}$ variant (Fig. 6b and Table S12). Though, adversely for the TAP2 protein, cancer-associated mutation which induces stability (Fig. 6a), there were higher protein–protein interactions found for mutant apo-systems (Fig. 6b and Table S12). These findings suggest that the cancer-associated mutations either induce stability or flexibility in the TAP1 or TAP2 proteins (in the absence of peptide) can unfavorably affect the TAP1-TAP2 complex, by forming a higher number of protein–protein interactions. The conformation dynamics of the TAP transporters in the $TAP1_{E446K/W}$ (446 aa is also positioned at the region presented to MHC I; Fig. 2g) systems suggest that, upon mutation, TAP_{NBD} domains lack the tilt movement, which results distortion in the opening of pore towards the cytosol, and the closed ER lumen conformation (Fig. 6c; left panel). $TAP1_{V437F}$ and $TAP1_{V437I}$ formed a closed ER lumen pore, whereas only $TAP1_{V437F}$ showed tilt movement of the TAP_{NBD} domain lacking the complete opening of the cytosolic pore.

The TAP2 mutations at position 370 belongs to the region where it can hinder movement of the helices (Fig. 5b) and also affect the pore opening towards the cytosol; $TAP2_{D370W}$ showed a distorted but open cytosolic pore with moderate tilt movement of the TAP_{NBD}, whereas the $TAP2_{D370N}$ lacked such conformation. Analysis of the structural behavior as well as the RMSDs suggest that $TAP2_{D370W}$ induces rigidity resulting in the opened cytosolic pore with moderate tilt TAP_{NBD} movement (Fig. 6c; right panel). For both $TAP2_{G208F}$ and $TAP2_{G208S}$ systems the tilt TAP_{NBD} movement is observed as well as the open cytosolic pore, however, it is closed toward the ER lumen (Fig. 6c). The mutations at the peptide binding region ($TAP1_{R372Q}$ and $TAP2_{R373H}$) have the tilt movement with the open cytosolic passage, but $TAP2_{R373H}$ lacks the ER lumen opening. Overall, mutations in TAP1 completely block both ER and cytosolic pores of the TAP transporter that may hinder the intake and evacuation of the peptides from cytosol-to-ER, whereas mutation in the TAP2 protein mainly blocks the ER lumen pore (Fig. 6c).

Protein-protein interactions with an occupancy $\geq$50% (from 100 ns) were identified in the studied mutated systems (Fig. S11). Comparing TAP1-TAP2 intermolecular binding residues from mutated systems with the wild-type, suggests that TAP1 residues E302, D357, and R639 are frequently involved in TAP2 binding for the mutated systems, but not in wild-type (Fig. S11). Except for the $TAP1_{E446K}$ system, TAP1 residues D306, E334, E443, and E446 were interacting with TAP2 in wild-type as well as in the mutated systems. Particularly, in the wild-type situation, the TAP1 E446 residue was involved in the binding with TAP2, which when E446K mutation hindered such an interaction. The mutated $TAP1_{E446K}$ and wild-type system lack common protein–protein interactions (Fig. S11). The R373 residue from TAP2 was traced in the majority of the mutated systems (Figs. 6 and S11) as well as wild-type binding with TAP1, excluding the $TAP2_{R373H}$ mutated system. Additionally, the TAP2 residues R235, E348, E349, Y366, Y366, and R381 binding with TAP1 were frequently traced in mutated systems (Fig. S11).

The direct consequences of cancer-associated variants over the peptide transport process by TAP heterodimer were evaluated by performing MD simulation of peptide in the presence of mutated TAP1-TAP2 complex. Both $TAP1_{R372Q}$ and $TAP2_{R373H}$ cancer-associated mutations are located in the peptide binding region and were involved in the interactions with peptides, hence were selected for MD simulations with two different peptides; pep18 and SIINFEKL (Fig. 2i). During the initial screen (Fig. 2i), pep18 peptide produced a strong binding affinity (−20.02 kcal/mol) with the TAP1-TAP2 complex but the SIINFEKL peptide (−13.44 kcal/mol) had comparatively weak affinity. The mutated TAP1 was found highly flexible compared to the mutated TAP2, and pep18 as well the variant residue $TAP1_{R372Q}$ itself were found destabilized (Fig. S12). Among mutated systems with peptide, the TAP1-SIINFEKL-$TAP2_{R373H}$ complex had a higher number of protein–protein interactions, and the $TAP1_{R372Q}$-pep18-TAP2 complex is the lowest to form such binding (Fig. 6d and Table S13). Comparing these protein–protein interactions from peptide bound mutated systems ($TAP1_{R372Q}$ and $TAP2_{R373H}$; Fig. 6d) with mutated apo-systems (Fig. 6b), the data suggest that peptide bound system has comparatively less TAP1-TAP2 intermolecular interactions.

Peptide-protein interactions suggest that both pep18 and SIINFEKL peptides formed a higher number of hydrogen bond interactions with the TAP2 protein, compared to that of the TAP1 (Fig. S12c and Table S14). Particularly, pep18 peptide formed more interactions with TAP1 protein in the $TAP1_{R372Q}$-pep18-TAP2 system (Fig. S12c). For the $TAP1_{R372Q}$ system, the SIINFEKL peptide formed H-bond with more number of residues having an occupancy $\geq$1 ns. The pep18 peptide and TAP1(E519) residue formed high occupancy interactions in the wild-type system (Fig. 5f), whereas lower occupancy binding with TAP1 is observed in the $TAP1_{R372Q}$ system (Fig. 6d). In addition, for the $TAP2_{R373H}$ system the SIINFEKL peptide had residues E417, R380, and R381 in common with the wild type and mutated systems (Fig. 5f and 6d), similarly the pep18 peptide formed interactions with R210, S421, R273, and N269 residues.

The area from the top of the TAP transport tunnel (towards the ER lumen; residues as described in Fig. 5b) for all four mutated systems with peptides (Fig. 6e), suggest a closed ER lumen conformation in the mutated complexes. For both peptides pep18 and SIINFEKL, the mutation in the $TAP1_{R372Q}$ and $TAP2_{R373H}$ blocks the movement of the peptide to upwards from cytosol-to-ER (Fig. 6f, g, S13, and Videos S4, S5), particularly the $TAP2_{R373H}$ residue was found interacting with pep18 peptide (Table S14). Distances between the peptide and the TAP residues from the top (ER lumen; Fig. 6f) demonstrated that, in the mutated $TAP1_{R372Q}$ and $TAP2_{R373H}$ systems, pep18 peptide has a higher distance value. Analysing the structural conformations of peptides in the presence of the mutation and wild type systems, the cancer-associated mutation induces rigidity in the TAP1-TAP2 complex, and hence, lacks an 'open' conformation towards the ER lumen. For an example (Figs. 6g, 7, S138, and Video S5), the movement of pep18 in the wild type as well as mutant system is shown, the peptide can shift upwards to the ER for the wild-type system, whereas for mutant the cavity pore is closed towards the ER lumen. For the opening of the cavity pore towards the ER in the wild-type system, a higher degree of conformations were observed in the TAP2 protein (Fig. 6g; left panel). Moreover, one shall also consider that mutations may have selection over each peptide, i.e., different cancers or the same cancer might have different mutations. Therefore, the mutational effect that blocks the movement of the peptide to upwards from cytosol-to-ER (Fig. 6g and S13) maybe seen in $TAP1_{R372Q}$ (found in cervical squamous cell carcinoma, colon adenocarcinoma, glioblastoma multiforme, and cervical squamous cell carcinoma) and $TAP2_{R373H}$ (found in prostate adenocarcinoma and glioblastoma multiforme).

4. Conclusions

Our work highlights the structural and functional insights into the molecular architecture of the peptide transit by the TAP1 and TAP2 transporters, and how cancer-derived mutations (from COS-

MIC and cBioPortal) as well as different viral factors (BNLF2a, CPXV012, ICP47, US6, and UL49.5) targeting TAP proteins may suppress the MHC class I pathway. This results in immune escape by the cancer and/or virus-carrying cell. To investigate the kinetics of the peptide transport process, different immunopeptidome datasets (MHC-I bound peptides presented by melanoma A375 cells) were generated in the presence/absence of interferon-γ treated samples to obtain peptide datasets for the TAP models, along with considering a set of peptides known to be presented on the TCR (from ATLAS database). Higher numbers of peptides were identified in the IFN-γ treated melanoma cells (3081 peptides) compared to that of the untreated cells (1968 peptides), suggesting an induced anti-cancer immunity pathway is being activated. These IFN-γ treated cells generated peptides with length of 8–10 mers that showed the binding affinity between −10 to −15 kcal/-mol (GBVI/WSA dG) with the modeled TAP1-TAP2 transporters. The majority of shorter length peptides from IFN-γ treated cells have less binding affinity with the TAP transporters. Exclusively in the IFN-γ treated cells the following peptides were identified from the TAP transporters itself; TAP1 (AALPAAALW, LLYESPERY, RSLQENIAY, RTALPRIF, SAMPTVRSF, and TEVDEAGSQL) and TAP2 (YLHSQVVSV). In addition, more residues from TAP2 were involved in interacting with the peptides, and fewer peptides were detected from TAP2 itself, whereas the opposite was observed for the TAP1.

Viral proteins predominantly destabilize the TAP1 protein, compared to that of the TAP2, particularly, for the UL49.5 and BNLF2a. Among the studied viral proteins, the UL49.5 protein exhibited the highest fluctuations and BNLF2a was the most stable protein. Interestingly, the peptides identified in the immunopeptidome data upon IFN-γ treated melanoma cells, originates from the highly fluctuating regions of the TAP transporters upon viral binding (or the allosteric effects). The structural dynamics of the TAP1-TAP2 complex in the presence and absence of a viral protein in the complex, revealed that in all simulated systems the TAP_{NBD} domains formed a tilt movement toward the membrane cytosolic face, which generates a passage or the peptide transport channel open towards the cytosol. This cytosolic passage was targeted by 4 (BNLF2a, CPXV012, ICP47, and UL49.5) out of 5 studied viral proteins. The BNLF2a, CPXV012, and ICP47 viral proteins formed a higher number of interactions with TAP1, whereas UL49.5 and US6 shared relatively equal interactions with both TAP proteins. In addition, the TAP1 regions with lower SNPs frequency and cancer variants were found making higher interactions with viral factors (proposing an adaptive mechanism, overcoming the protein–protein interactions that might result from amino acid changes), whereas the viral protein binds to the TAP2 region which is highly mutated. Exceptionally, the US6 protein has unique interactions with the transporters, whereas other BNLF2a/CPXV012/ICP47/UL49.5 viral factors have several amino acids in common when binding with the TAP proteins.

Individual amino acid fluctuations for the TAP proteins suggest that presence of shorter peptides (pep20 and SIINFEKL) induced stability in the transporter, compared to longer peptide (pep18). TAP self peptides or regions from the immunopeptidome showing higher flexibility in viral systems, lacked such behavior in the peptide-bound systems. The structural movements of the cavity formed by the TAP transporters open towards the ER lumen, which may be proposed to transport the peptides from cytosol-to-ER in two different ways via an opening of the tunnel (4 or 8 helices involvement). Particularly, for the SIINFEKL (8-mer), which is smaller in length compared to that of the pep18 (15-mer), only the one passage formed by two helices from each TAP1 and TAP2 was found open, whereas for pep18 both passages, or areas, formed by 8 helices (4 from each TAP1 and TAP2) were in the open state. However, such difference in the opening of the passage towards the ER lumen may also vary based on the peptide sequences. The distance measured for each peptide from the top of the TAP models towards the ER lumen suggests that a shorter peptide (SIINFEKL) has an initiated movement relatively earlier compared to the longer peptide (pep18). At a point when the TAP1-TAP2 cavity is in its open conformation towards the ER, and the peptide reaches the top of the transport tunnel it mainly interacts with the TAP2 protein. The S203, Q388, and M413 amino acids from the TAP2 proteins were found common in at least two peptide systems. Similar as that observed in the EPR studies, a conserved distance of about 25 Å between the N and C terminus of the peptides bound with TAP proteins was observed in our analysis; the 15-mer (pep18) has a distance of 37.38 Å, the 9-mer (pep20) has 21.57 Å distance, and 8-mer (SIINFEKL) has 21.92 Å distance.

The TAP1 or TAP2 amino acids binding with peptides in fingerprint analysis, were also found mutated in different cancer types, which suggest that point mutation either from TAP1 or TAP2 is sufficient to alter the protein–protein binding which may affect the peptide transport process. Interestingly, the variants located at the peptide binding pocket of the TAP1-TAP2 complex have diverse conformations; the $TAP1_{R372Q}$ variant was found highly stable compared to that of the $TAP2_{R373H}$. The mutations in TAP1 may completely block both ER and cytosolic passage of the TAP transporter which may hinder the intake and evacuation of the peptides from cytosol-to-ER (blocks the IF-to-OF conformation), whereas mutation in the TAP2 protein mostly blocks the ER pore only. The mutated system TAP1-SIINFEKL-$TAP2_{R373H}$ had a higher number of protein–protein interactions, and the $TAP1_{R372Q}$-pep18-TAP2 complex is one of the lowest to form such binding. Considering both pep18 and SIINFEKL peptides, the mutation in the $TAP1_{R372Q}$ and $TAP2_{R373H}$ blocks the movement of the peptide upwards in the transport channel. For the opening of the transport cavity pore towards the ER lumen in the wild-type system, a higher degree of conformations is observed in the TAP2 protein, whereas the structural conformations of peptides in the presence of the mutation systems suggest that the cancer mutation induces rigidity in the TAP1-TAP2 complex, and therefore, lacks the 'open' conformation towards the ER lumen.

Overall, considering the binding affinities of the peptide with transporters it could be proposed that smaller peptides (8, 9, or 10 mers) may transport comparatively quickly through the transport channel. Furthermore, by adversely interacting with the TAP transport passage, or affecting the TAP_{NBD} tilt movement, viral proteins and cancer-derived mutations may induce allosteric effects or rigidity in the TAP complex blocking the IF-to-OF conformation of the tunnel. The areas from the TAP transporter towards ER-opening and the distance centre of mass between TAP_{NBD} domains, highlights a difference in the transport of longer vs shorter peptides. However, the sequence composition of peptide can affect the rate of such conformations by the transporters. These findings would propose a model for how different viral factors and cancer-derived mutations alter the peptide transport process by directly targeting the TAP proteins, and how the IFN-γ induced signaling pathway alters TAP-peptide loading and, ultimately, MHC-I antigen presentation.

Funding

The APC was funded by the International Centre for Cancer Vaccine Science, University of Gdansk (Fundacja na rzecz Nauki Polskiej: MAB/3/2017). U.K. is supported by the grant: 2020/36/C/NZ2/00108, from The National Science Centre (Narodowe Centrum Nauki, Krakow, Poland). Partly funded by European Regional Development Fund (ENOCH, CZ.02.1.01/0.0/0.0/16_019/0000868), MH CZ – DRO (MMCI, 00209805), CancerforskningsfondenNorr, Cancerfonden (160598).

Declaration of Competing Interest

The authors declare that they have no known competing financial interests or personal relationships that could have appeared to influence the work reported in this paper.

Acknowledgments

The International Centre for Cancer Vaccine Science project is carried out within the International Research Agendas programme of the Foundation for Polish Science co-financed by the European Union under the European Regional Development Fund. Authors would also like to thank the PL-Grid Infrastructure, Poland for providing their hardware and software resources.

Appendix A. Supplementary data

Supplementary data to this article can be found online at https://doi.org/10.1016/j.csbj.2021.09.006.

References

[1] Praest P, Liaci AM, Förster F, Wiertz EJHJ. New insights into the structure of the MHC class I peptide-loading complex and mechanisms of TAP inhibition by viral immune evasion proteins. Mol Immunol 2019;113:103–14.
[2] Sadasivan B, Lehner PJ, Ortmann B, Spies T, Cresswell P. Roles for calreticulin and a novel glycoprotein, tapasin, in the interaction of MHC class I molecules with TAP. Immunity 1996;5(2):103–14.
[3] Park B, Lee S, Kim E, Cho K, Riddell SR, Cho S, et al. Redox regulation facilitates optimal peptide selection by MHC class I during antigen processing. Cell 2006;127(2):369–82.
[4] Stefková J, Poledne R, Hubácek JA. ATP-binding cassette (ABC) transporters in human metabolism and diseases. Physiol Res 2004;53:235–43.
[5] Perria CL, Rajamanickam V, Lapinski PE, Raghavan M. Catalytic site modifications of TAP1 and TAP2 and their functional consequences. J Biol Chem 2006;281(52):39839–51.
[6] Parcej D, Tampé R (2010) ABC proteins in antigen translocation and viral inhibition. Nat Chem Biol 6: 572-580 Erratum in: (2010) Nat Chem Biol 6: 782.
[7] Dean M, Annilo T. Evolution of the ATP-binding cassette (ABC) transporter superfamily in vertebrates. Annu Rev Genomics Hum Genet 2005;6 (1):123–42.
[8] Lehnert E, Tampé R. Structure and dynamics of antigenic peptides in complex with TAP. Front Immunol 2017;8:10.
[9] Marijt KA, van Hall T. To TAP or not to TAP: alternative peptides for immunotherapy of cancer. Curr Opin Immunol 2020;64:15–9.
[10] van Endert PM, Tampé R, Meyer TH, Tisch R, Bach J-F, McDevitt HO. A sequential model for peptide binding and transport by the transporters associated with antigen processing. Immunity 1994;1(6):491–500.
[11] Uebel S, Meyer TH, Kraas W, Kienle S, Jung G, Wiesmller K-H, et al. Requirements for peptide binding to the human transporter associated with antigen processing revealed by peptide scans and complex peptide libraries. J Biol Chem 1995;270(31):18512–6.
[12] Neefjes JJ, Momburg F, Hämmerling GJ (1993) Selective and ATP-dependent translocation of peptides by the MHC-encoded transporter. Science 261: 769-771 Erratum in: (1994) Science 264: 16.
[13] Seyffer F, Tampé R. ABC transporters in adaptive immunity. Biochim Biophys Acta 2015;1850(3):449–60.
[14] Locher KP. Mechanistic diversity in ATP-binding cassette (ABC) transporters. Nat Struct Mol Biol 2016;23(6):487–93.
[15] Eggensperger S, Tampé R. The transporter associated with antigen processing: a key player in adaptive immunity. Biol Chem 2015;396:1059–72.
[16] Abele R, Tampé R (2011) The TAP translocation machinery in adaptive immunity and viral escape mechanisms. Essays Biochem 50: 249-264.
[17] Mayerhofer PU, Tampé R. Antigen translocation machineries in adaptive immunity and viral immune evasion. J Mol Biol 2015;427(5):1102–18.
[18] Oldham ML, Hite RK, Steffen AM, Damko E, Li Z, Walz T, et al. A mechanism of viral immune evasion revealed by cryo-EM analysis of the TAP transporter. Nature 2016;529(7587):537–40.
[19] Lankat-Buttgereit B, Tampé R. The transporter associated with antigen processing: function and implications in human diseases. Physiol Rev 2002;82(1):187–204.
[20] Ljunggren H-G, Stam NJ, Öhlén C, Neefjes JJ, Höglund P, Heemels M-T, et al. Empty MHC class I molecules come out in the cold. Nature 1990;346 (6283):476–80.
[21] Praest P, Luteijn RD, Brak-Boer IGJ, Lanfermeijer J, Hoelen H, Ijgosse L, et al. The influence of TAP1 and TAP2 gene polymorphisms on TAP function and its inhibition by viral immune evasion proteins. Mol Immunol 2018;101:55–64.
[22] Yewdell JW, Bennink JR. Mechanisms of viral interference with MHC class I antigen processing and presentation. Annu Rev Cell Dev Biol 1999;15 (1):579–606.
[23] Oldham ML, Grigorieff N, Chen J (2016) Structure of the transporter associated with antigen processing trapped by herpes simplex virus. Elife 5: e21829.
[24] McLaughlin-Drubin ME, Munger K. Viruses associated with human cancer. Biochim Biophys Acta 2008;1782(3):127–50.
[25] Ritz U, Seliger B. The transporter associated with antigen processing (TAP): structural integrity, expression, function, and its clinical relevance. Mol Med 2001;7(3):149–58.
[26] Hicklin DJ, Marincola FM, Ferrone S. HLA class I antigen downregulation in human cancers: T-cell immunotherapy revives an old story. Mol Med Today 1999;5(4):178–86.
[27] Marincola FM, Jaffee EM, Hicklin DJ, Ferrone S. Escape of human solid tumors from T-cell recognition: molecular mechanisms and functional significance. Adv Immunol 2000;74:181–273.
[28] Seliger B, Maeurer MJ, Ferrone S. TAP off–tumors on. Immunol Today 1997;18:292–9.
[29] Verweij MC, Horst D, Griffin BD, Luteijn RD, Davison AJ, Ressing ME, et al. Viral inhibition of the transporter associated with antigen processing (TAP): a striking example of functional convergent evolution. PLoS Pathog 2015;11(4): e1004743.
[30] Vossen M, Westerhout E, Söderberg-Nauclér C, Wiertz E. Viral immune evasion: a masterpiece of evolution. Immunogenetics 2002;54(8):527–42.
[31] Tashiro H, Brenner MK. Immunotherapy against cancer-related viruses. Cell Res. 2017;27(1):59–73.
[32] Hislop AD, Ressing ME, van Leeuwen D, Pudney VA, Horst D et al. (2007) A CD8+ T cell immune evasion protein specific to Epstein-Barr virus and its close relatives in Old World primates. J Exp Med 204: 1863–73.
[33] Alzhanova D, Edwards DM, Hammarlund E, Scholz IG, Horst D, Wagner MJ, et al. Cowpox virus inhibits the transporter associated with antigen processing to evade T cell recognition. Cell Host Microbe 2009;6 (5):433–45.
[34] Hill A, Jugovic P, York L, Russ G, Bennink J, Yewdell J, et al. Herpes simplex virus turns off the TAP to evade host immunity. Nature 1995;375 (6530):411–5.
[35] Früh K, Ahn K, Djaballah H, Sempé P, van Endert PM, Tampé R, et al. A viral inhibitor of peptide transporters for antigen presentation. Nature 1995;375 (6530):415–8.
[36] Hewitt EW, Gupta SS, Lehner PJ. The human cytomegalovirus gene product US6 inhibits ATP binding by TAP. EMBO J 2001;20:387–96.
[37] Koppers-Lalic D, Reits EAJ, Ressing ME, Lipinska AD, Abele R, Koch J, et al. Varicelloviruses avoid T cell recognition by UL49.5-mediated inactivation of the transporter associated with antigen processing. Proc Natl Acad Sci U S A 2005;102(14):5144–9.
[38] Loch S, Tampé R. Viral evasion of the MHC class I antigen-processing machinery. Pflugers Arch 2005;451(3):409–17.
[39] Schuren ABC, Costa AI, Wiertz EJHJ. Recent advances in viral evasion of the MHC class I processing pathway. Curr Opin Immunol 2016;40:43–50.
[40] Komov L, Melamed Kadosh D, Barnea E, Admon A. The effect of interferons on presentation of defective ribosomal products as HLA peptides. Mol Cell Proteomics 2021;20:100105.
[41] García-Sastre A. Ten strategies of interferon evasion by viruses. Cell Host Microbe 2017;22(2):176–84.
[42] Padariya M, Sznarkowska A, Kote S, Gómez-Herranz M, Mikac S, Pilch M, et al. Functional interfaces, biological pathways, and regulations of interferon-related DNA damage resistance signature (IRDS) genes. Biomolecules 2021;11(5):622.
[43] Herget M, Baldauf C, Scholz C, Parcej D, Wiesmuller K-H, Tampe R, et al. Conformation of peptides bound to the transporter associated with antigen processing (TAP). Proc Natl Acad Sci U S A 2011;108(4):1349–54.
[44] Saric T, Chang SC, Hattori A, York IA, Markant S, et al. An IFN-gamma-induced aminopeptidase in the ER, ERAP1, trims precursors to MHC class Ipresented peptides. Nat Immunol 2002;3:1169–76.
[45] Zhou F. Molecular mechanisms of IFN-γ to up-regulate MHC class I antigen processing and presentation. Int Rev Immunol 2009;28(3-4):239–60.
[46] Strehl B, Seifert U, Kruger E, Heink S, Kuckelkorn U, Kloetzel P-M. Interferongamma, the functional plasticity of the ubiquitin-proteasome system, and MHC class I antigen processing. Immunol Rev 2005;207 (1):19–30.
[47] Arellano-Garcia ME, Misuno K, Tran SD, Hu S, van Hall T. Interferon-γ induces immunoproteasomes and the presentation of MHC I-associated peptides on human salivary gland cells. PLoS ONE 2014;9(8):e102878.
[48] Borrman T, Cimons J, Cosiano M, Purcaro M, Pierce BG, Baker BM, et al. ATLAS: A database linking binding affinities with structures for wild-type and mutant TCR-pMHC complexes. Proteins 2017;85(5):908–16.
[49] Natter C, Polterauer S, Rahhal-Schupp J, Cacsire Castillo-Tong D, Pils S, Speiser P, et al. Association of TAP gene polymorphisms and risk of cervical intraepithelial neoplasia. Dis Markers 2013;35:79–84.
[50] Einstein MH, Leanza S, Chiu LG, Schlecht NF, Goldberg GL, Steinberg BM, et al. Genetic variants in TAP are associated with high-grade cervical neoplasia. Clin Cancer Res 2009;15(3):1019–23.
[51] Abele R, Tampé R. The ABCs of immunology: structure and function of TAP, the transporter associated with antigen processing. Physiology (Bethesda) 2004;19(4):216–24.

[52] Ozbas-Gerceker F, Bozman N, Gezici S, Pehlivan M, Yilmaz M, Pehlivan S, et al. Association of TAP1 and TAP2 gene polymorphisms with hematological malignancies. Asian Pac J Cancer Prev 2013;14(9):5213–7.
[53] Henle AM, Nassar A, Puglisi-Knutson D, Youssef B, Knutson KL, Ahmad A. Downregulation of TAP1 and TAP2 in early stage breast cancer. PLoS ONE 2017;12(11):e0187323.
[54] Forbes SA, Beare D, Boutselakis H, Bamford S, Bindal N, Tate J, et al. COSMIC: somatic cancer genetics at high-resolution. Nucleic Acids Res 2017;45(D1): D777–83.
[55] Cerami E, Gao J, Dogrusoz U, Gross BE, Sumer SO et al. (2012) The cBio cancer genomics portal: an open platform for exploring multidimensional cancer genomics data. Cancer Discov 2: 401–404 Erratum in: (2012) Cancer Discov 2: 960.
[56] Grotzke JE, Sengupta D, Lu Q, Cresswell P. The ongoing saga of the mechanism (s) of MHC class I-restricted cross-presentation. Curr Opin Immunol 2017;46:89–96.
[57] Merzougui N, Kratzer R, Saveanu L, van Endert P. A proteasome-dependent, TAP-independent pathway for cross-presentation of phagocytosed antigen. EMBO Rep 2011;12(12):1257–64.
[58] Lawand M, Abramova A, Manceau V, Springer S, van Endert P. TAP-dependent and -independent peptide import into dendritic cell phagosomes. J Immunol 2016;197(9):3454–63.
[59] Karplus M, McCammon JA (2002) Molecular dynamics simulations of biomolecules. Nat Struct Biol 9: 646–52 Erratum in: (2002) Nat Struct Biol 9: 788.
[60] Faktor J, Grasso G, Zavadil Kokas F, Kurkowiak M, Mayordomo MY, Kote S, et al. The effects of p53 gene inactivation on mutant proteome expression in a human melanoma cell model. Biochim Biophys Acta Gen Subj 2020;1864 (12):129722.
[61] Lanoix J, Durette C, Courcelles M, Cossette É, Comtois-Marotte S, et al. Comparison of the MHC I immunopeptidome repertoire of B-cell lymphoblasts using two isolation methods. Proteomics 2018;18:e1700251.
[62] Cox J, Matic I, Hilger M, Nagaraj N, Selbach M, Olsen JV, et al. A practical guide to the MaxQuant computational platform for SILAC-based quantitative proteomics. Nat Protoc 2009;4(5):698–705.
[63] Cox J, Hein MY, Luber CA, Paron I, Nagaraj N, Mann M. Accurate proteome-wide label-free quantification by delayed normalization and maximal peptide ratio extraction, termed MaxLFQ. Mol Cell Proteomics 2014;13(9):2513–26.
[64] Tyanova S, Temu T, Cox J. The MaxQuant computational platform for mass spectrometry-based shotgun proteomics. Nat Protoc 2016;11(12):2301–19.
[65] Cox Jürgen, Neuhauser N, Michalski A, Scheltema RA, Olsen JV, Mann M. Andromeda: a peptide search engine integrated into the MaxQuant environment. J Proteome Res 2011;10(4):1794–805.
[66] Kelley LA, Sternberg MJE. Protein structure prediction on the web: a case study using the Phyre server. Nat Protoc 2009;4(3):363–71.
[67] Kelley LA, Mezulis S, Yates CM, Wass MN, Sternberg MJE. The Phyre2 web portal for protein modeling, prediction and analysis. Nat Protoc 2015;10 (6):845–58.
[68] Molecular Operating Environment (MOE) 2011.10. Chemical Computing Group (2011) Montreal, Quebec, Canada.
[69] Brooks BR, Brooks CL, Mackerell AD, Nilsson L, Petrella RJ, Roux B, et al. CHARMM: the biomolecular simulation program. J Comput Chem 2009;30 (10):1545–614.
[70] Labute P. The generalized Born/volume integral implicit solvent model: estimation of the free energy of hydration using London dispersion instead of atomic surface area. J Comput Chem 2008;29(10):1693–8.
[71] Krivák R, Hoksza D. Improving protein-ligand binding site prediction accuracy by classification of inner pocket points using local features. J Cheminform 2015;7:12.
[72] Kitchen DB, Decornez H, Furr JR, Bajorath J. Docking and scoring in virtual screening for drug discovery: methods and applications. Nat Rev Drug Discov 2004;3(11):935–49.
[73] Wojciechowski M, Lesyng B. Generalized Born model: Analysis, refinement, and applications to proteins. J Phys Chem B 2004;108:18368–76.
[74] Labute P. LowModeMD–implicit low-mode velocity filtering applied to conformational search of macrocycles and protein loops. J Chem Inf Model 2010;50(5):792–800.
[75] Karczewski KJ, Francioli LC, Tiao G, Cummings BB, Alföldi J et al. (2020) The mutational constraint spectrum quantified from variation in 141,456 humans. Nature 581: 434–43 Erratum in: (2021) Nature 590: E53.
[76] Lomize MA, Pogozheva ID, Joo H, Mosberg HI, Lomize AL (2012) OPM database and PPM web server: resources for positioning of proteins in membranes. Nucleic Acids Res 40: D370–D376.
[77] Jo S, Lim JB, Klauda JB, Im W. CHARMM-GUI Membrane Builder for mixed bilayers and its application to yeast membranes. Biophys J 2009;97(1):50–8.
[78] Trowitzsch S, Tampé R. Multifunctional chaperone and quality control complexes in adaptive immunity. Annu Rev Biophys 2020;49(1):135–61.
[79] Loschwitz J, Olubiyi OO, Hub JS, Strodel B, Poojari CS. Computer simulations of protein-membrane systems. Prog Mol Biol Transl Sci 2020;170:273–403.
[80] Woolf TB, Roux B. Structure, energetics, and dynamics of lipid-protein interactions: A molecular dynamics study of the gramicidin A channel in a DMPC bilayer. Proteins 1996;24(1):92–114.
[81] Phillips JC, Braun R, Wang W, Gumbart J, Tajkhorshid E, Villa E, et al. Scalable molecular dynamics with NAMD. J Comput Chem 2005;26(16):1781–802.
[82] Klauda JB, Venable RM, Freites JA, O'Connor JW, Tobias DJ, Mondragon-Ramirez C, et al. Update of the CHARMM all-atom additive force field for lipids: validation on six lipid types. J Phys Chem B 2010;114(23):7830–43.
[83] Venable RM, Brown FLH, Pastor RW. Mechanical properties of lipid bilayers from molecular dynamics simulation. Chem Phys Lipids 2015;192:60–74.
[84] Guvench O, Mallajosyula SS, Raman EP, Hatcher E, Vanommeslaeghe K, Foster TJ, et al. CHARMM additive all-atom force field for carbohydrate derivatives and its utility in polysaccharide and carbohydrate-protein modeling. J Chem Theory Comput 2011;7(10):3162–80.
[85] Jorgensen WL, Chandrasekhar J, Madura JD, Impey RW, Klein ML. Comparison of simple potential functions for simulating liquid water. J Chem Phys 1983;79(2):926–35.
[86] Darden T, York D, Pedersen L. Particle mesh Ewald- an N · log(N) method for Ewald sums in large systems. J Chem Phys 1993;98(12):10089–92.
[87] Pastor RW, Brooks BR, Szabo A. An analysis of the accuracy of langevin and molecular dynamics algorithms. Mol Phys 1988;65(6):1409–19.
[88] Feller SE, Zhang Y, Pastor RW, Brooks BR. Constant pressure molecular dynamics simulation: the Langevin piston method. J Chem Phys 1995;103 (11):4613–21.
[89] Ryckaert JP, Ciccotti G, Berendsen HJC. Numerical integration of cartesian equations of motion of a system with constraints: molecular dynamics of n-alkanes. J Comput Phys 1977;23:327–41.
[90] Humphrey W, Dalke A, Schulten K. VMD: visual molecular dynamics. J Mol Graph 1996;14(1):33–8.
[91] Rock KL, Goldberg AL. Degradation of cell proteins and the generation of MHC class I-presented peptides. Annu Rev Immunol 1999;17(1):739–79.
[92] Stryhn A, Pedersen L, Holm A, Buus S. Longer peptide can be accommodated in the MHC class I binding site by a protrusion mechanism. Eur J Immunol 2000;30(11):3089–99.
[93] Guo H-C, Jardetzky TS, Garrettt TPJ, Lane WS, Strominger JL, Wiley DC. Different length peptides bind to HLA-Aw68 similarly at their ends but bulge out in the middle. Nature 1992;360(6402):364–6.
[94] Urban RG, Chicz RM, Lane WS, Strominger JL, Rehm A, Kenter MJ, et al. A subset of HLA-B27 molecules contains peptides much longer than nonamers. Proc Natl Acad Sci U S A 1994;91(4):1534–8.
[95] Rock KL, Reits E, Neefjes J. Present yourself! By MHC class I and MHC class II molecules. Trends Immunol 2016;37(11):724–37.
[96] Koopmann JO, Post M, Neefjes JJ, Hämmerling GJ, Momburg F. Translocation of long peptides by transporters associated with antigen processing (TAP). Eur J Immunol 1996;26(8):1720–8.
[97] Kisselev AF, Akopian TN, Woo KM, Goldberg AL. The size of peptides generated from proteins by mammalian 26 and 20S proteasomes. J Biol Chem 1999;274:3363–71.
[98] Nogales A, L. DeDiego M. Host single nucleotide polymorphisms modulating influenza A virus disease in humans. Pathogens 2019;8(4):168.
[99] Bordignon E, Seeger MA, Galazzo L, Meier G. From in vitro towards in situ: structure-based investigation of ABC exporters by electron paramagnetic resonance spectroscopy. FEBS Lett 2020;594:3839–56.
[100] Hofmann S, Januliene D, Mehdipour AR, Thomas C, Stefan E, Brüchert S, et al. Conformation space of a heterodimeric ABC exporter under turnover conditions. Nature 2019;571(7766):580–3.
[101] Stefan E, Hofmann S, Tampé R. A single power stroke by ATP binding drives substrate translocation in a heterodimeric ABC transporter. eLife 2020;9: e55943.
[102] Nöll A, Thomas C, Herbring V, Zollmann T, Barth K, Mehdipour AR, et al. Crystal structure and mechanistic basis of a functional homolog of the antigen transporter TAP. Proc Natl Acad Sci U S A 2017;114(4):E438–47.
[103] Armandola EA, Momburg F, Nijenhuis M, Bulbuc N, Früh K, Hämmerling GJ. A point mutation in the human transporter associated with antigen processing (TAP2) alters the peptide transport specificity. Eur J Immunol 1996;26 (8):1748–55.
[104] Denton AE, Wesselingh R, Gras S, Guillonneau C, Olson MR, Mintern JD, et al. Affinity thresholds for naive CD8+ CTL activation by peptides and engineered influenza A viruses. J Immunol 2011;187(11):5733–44.
[105] Sethi DK, Schubert DA, Anders AK, Heroux A, Bonsor, DA et al. (2011) A highly tilted binding mode by a self-reactive T cell receptor results in altered engagement of peptide and MHC. J Exp Med 208: 91–102.
[106] Borbulevych OY, Santhanagopolan SM, Hossain M, Baker BM. TCRs used in cancer gene therapy cross-react with MART-1/Melan-A tumor antigens via distinct mechanisms. J Immunol 2011;187(5):2453–63.